UNIVERSITY OF TWENTE.

Faculty of Engineering Technology,
Dynamics Based Maintenance

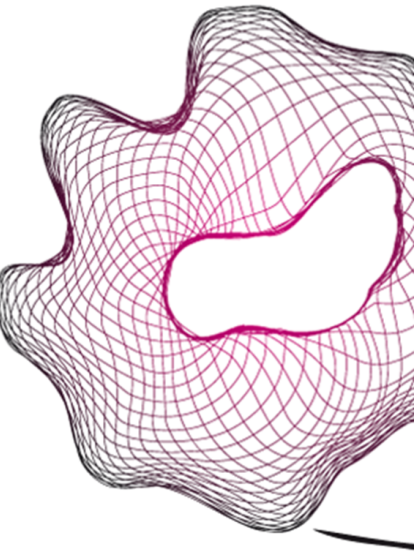

Development of a Diagnostic Tool based on Continuous Scanning LDV Output Spectra

Sietze Bruinsma

Master Thesis
October 2018

Examination committee:
prof. dr. ir. T. Tinga
dr. D. Di Maio
dr. ir. R.G.K.M. Aarts

Development of a Diagnostic Tool based on Continuous Scanning LDV Output Spectra

Master Thesis

Sietze Bruinsma
s1356666

Enschede, The Netherlands
15-10-2018

University of Twente
Faculty of Engineering Technology
Mechanical Engineering
Dynamics Based Maintenance

Supervisors:
DR. Dario Di Maio
PROF.DR.IR. Tiedo Tinga
External member:
DR.IR. Ronald G.K.M. Aarts

Preface

This thesis is the result of my masters assignment for the Dynamics Based Maintenance chair of the Mechanical Engineering master at the University of Twente. In this thesis I defined my own damage indicator that can be used for structural health monitoring.
I hope this paper illustrates my work in an understandable way and that it will be used as reference for further studies.

First of all, I would like to thank Dario for his incredible supervision and support. From the very start you showed your confidence in me and the research, which I greatly appreciated. You encouraged me to present my work at the 13th A.I.VE.LA. conference in Ancona, Italy. I am honoured to have presented the research there. I would also like to thank Tiedo for making the trip to the conference possible and for the guidance during this 10 month project.

Finally I thank my family and friends for the moral, financial and/or literal support. I really appreciated you all listening to me ramble on about my study progress.

Sietze Bruinsma
Enschede, 28 September 2018

Summary

This thesis presents a study on a novel diagnostics method for use in dynamics based maintenance. Structural Health Monitoring (SHM) is becoming an essential part of maintenance strategies. The demand from the industry for better diagnostic tools is on the rise. A fast, non-contact and non-destructive measurement device based on scanning laser vibrometry can be used for damage detection methodologies. Early detection of damage, or deterioration of stiffness, in operating conditions is key in determining the expected remaining lifetime of the system.
Continuous Scanning Laser Doppler Vibrometry (CSLDV) measures the vibration response of a component remotely, obtaining spatial and temporal information in seconds. It can be used as a powerful and rapid approach to damage detection in operating conditions.
This thesis describes the development of a diagnostic tool using the output spectra of the CSLDV method. The focus of the study lies on cantilever structures, where one end of a beam is clamped, and the other end is subjected to an excitation force. A two dimensional numerical study is undertaken, in which multiple cases of different damage types and severities are simulated. The frequency responses in a range up to 9000 Hz are investigated. The nodal responses of the scanned line are obtained from the simulation and the output time signal of the CSLDV method is simulated. At every frequency a discrete Fast Fourier Transform (dFFT) of the time signal yields a characteristic frequency spectrum. This spectrum consists of sidebands that carry spatial information of the deflection shape for that excitation frequency. The introduction of damage to the system changes the strain energy distribution over the beam, altering the dynamic behaviour at that specific frequency. Observing the dFFT spectrum at that frequency reveals that the sideband amplitudes have changed for the damage case with respect to the Pristine case.
A damage indicator is defined to gauge the deviation in the frequency spectrum as a result of the damage. The indicator should be robust, independent of the excitation force. The damage criterion is calculated by assigning a percentage to the contribution of the spectral sidebands to the summation of all the sidebands in that spectrum. This method is named the RASTAR method, Relative Amplitude of the Sidebands to the Total Amplitude Reference. The indicator behaves as expected; a more severe damage case yields a higher indicator value. The strain analysis suggested that the anti-resonances might be more sensitive to the damage than the eigen-frequencies, this is also seen in the numerical results. The deflection shape of the anti-resonance seems to imply an additional constraint that influences the strain energy distribution. Which in turn affects the spectrum.
An experimental analysis was performed on an aluminium beam. Two damage severities were applied and compared to the pristine case. The experiments are conducted up to 1000 Hz to obtain the highest signal-to-noise ratio. The general behaviour of the indicator is as expected; the larger damage resulted in a higher indicator value. The RASTAR method was able to detect a damage of 1x1x30 mm in a 400x10x30 mm beam.

Samenvatting

Dit rapport presenteert een onderzoek naar een nieuwe methode voor diagnose voor gebruik in op dynamica gebaseerd onderhoud. Structureel gezondheidsmonitoring (SHM) begint een essentieel onderdeel te worden van nieuwe onderhoudsstrategieën. De vraag naar betere methoden voor diagnose vanuit de industrie stijgt. Een snel, contactloos en niet-destructief meetapparaat gebaseed op laser vibratiemeting kan toegepast worden in schade opsporingsmethodes. Vroege ontdekking van schade, ook wel de achteruitgang van de stijfheid, in bedrijfsomstandigheden is belangrijk voor het vaststellen van de verwachte levensduur van het systeem.
'Continuous Scanning Laser Doppler Vibrometry' (CSLDV) haalt in seconden de ruimte en tijd informatie uit de trillingsreactie van een component op afstand. Het is een krachtige en snelle aanpak voor het opsporen van schade in een component gedurende bedrijfsomstandigheden.
Dit rapport beschrijft de ontwikkeling van een diagnose gereedschap die gebruik maakt van de spectra resulterend uit de CSLDV methode. De focus van het rapport ligt op ingeklemde constructies, waar één uiteinde van de balk is ingeklemd en één uiteinde is onderworpen aan een excitatiekracht. Een tweedimensionale numerieke studie is uitgevoerd, waarin meerdere verschillende dieptes en soorten schaden zijn gesimuleerd. De trillingsreacties van frequenties tot 9000 Hz zijn onderzocht. De beweging van de knooppunten in het model op de scanlijn zijn verzameld en het tijdssignaal van de CSLDV methode is gesimuleerd. Een discrete snelle Fouriertransformatie (dFFT) van het tijdssignaal resulteert in een karakteristiek frequentiespectrum voor elke frequentie. Dit spectrum bestaat uit zogenaamde 'sidebands', deze dragen de ruimtelijke informatie over de trillingsvorm voor die frequentie. Wanneer schade wordt geintroduceert aan het systeem veranderd de rek energie verdeling over de balk, wat het dynamisch gedrag voor deze specifieke frequentie veranderd. Het dFFT spectrum voor deze frequentie, met schade, is veranderd ten opzichte van deze frequentie zonder schade.
Een schade criterium is gedefinieerd om de verandering in het frequentiespectrum door de introductie van schade te meten. Het criterium moet robuust zijn en onafhankelijk van de hoogte van de excitatiekracht. Het criterium is berekend door de sidebands uit te drukken in een percentage van de som van alle sidebands in dat spectrum. De methode heet de RASTAR methode, naar Relative Amplitude of the Sidebands to the Total Amplitude Reference. Deze schade-indicator vertoont het verwachte gedrag; een zwaardere schade levert een hogere waarde in de indicator op. De analyse van het rek gedrag suggereerd dat de anti-resonantie gevoeliger is voor de schade dan de eigenfrequentie. Dit blijkt ook uit de numerieke resultaten. De trillingsvorm van de anti-resonantie lijkt een extra beperking op te leggen welke invloed heeft op de rek energieverdeling over de balk. Dit heeft vervolgens effect op het spectrum.
Een experimentele analyse van een aluminium balk is uitgevoerd. Twee zwaartes van schade zijn aangebracht op de balk en vergeleken met de meting van de nog intacte balk. De experimenten zijn ondernomen tot 1000 Hz voor een zo hoog mogelijke signaal-ruis ratio. Het algemene gedrag van criterium is zoals verwacht; de zwaardere schade resulteerde in een hogere waarde van de schade-indicator. De RASTAR methode is in staat om een schade van 1x1x30 mm te detecteren op een balk van 400x10x30 mm.

Nomenclature

CSLDV	Continuous Scanning Laser Doppler Vibrometry
dFFT	discrete Fast Fourier Transform
DOF	Degrees Of Freedom
FEA	Finite Element Analysis
FEM	Finite Element Method
FFT	Fast Fourier Transform
FRF	Frequency Response Function
LDV	Laser Doppler Vibrometry
MAC	Modal Assurance Criterion
MSE	Mean Square Error
ODS	Operational Deflection Shape
RASTAR	Relative Amplitude of the Sidebands to the Total Amplitude Reference
SBA	Sideband Amplitude
SHM	Structural Health Monitoring
SLDV	Scanning Laser Doppler Vibrometry

Damage Designations

D10L	10 Percent Longitudinal Damage case
D25L	25 Percent Longitudinal Damage case
D50L	50 Percent Longitudinal Damage case
D10T	10 Percent Transverse Damage case
D25T	25 Percent Transverse Damage case
D50T	50 Percent Transverse Damage case

Contents

Preface i

Summary ii

Samenvatting iii

Nomenclature iv

1 Introduction 1
- 1.1 Goal of the study . . . 1
- 1.2 Outline of the study . . . 2

2 Background 3
- 2.1 Detection techniques . . . 3
  - 2.1.1 Contact methods . . . 3
  - 2.1.2 Non-contact methods . . . 3
- 2.2 Theory on scanning laser vibrometry (CSLDV) . . . 4
- 2.3 Implications for the present work . . . 6

3 Numerical Study 7
- 3.1 Finite element model . . . 7
  - 3.1.1 Specification on element configuration . . . 7
  - 3.1.2 Damage typology . . . 9
  - 3.1.3 Final model configuration . . . 10
- 3.2 Strain Analysis . . . 10
  - 3.2.1 ODS comparison between pristine and damage case . . . 10
  - 3.2.2 Sensitivity of dynamic behaviour to the damage . . . 12
  - 3.2.3 Identification strategy . . . 14
- 3.3 Simulation of output spectrum using CSLDV method . . . 15
  - 3.3.1 Damage severity based on Frequency Response Function . . . 15
  - 3.3.2 Operational Deflection Shape definition . . . 17
  - 3.3.3 CSLDV output signal using ODS . . . 17

4 Damage indicator definitions 20
- 4.1 Development of damage indicators . . . 20
  - 4.1.1 Fingerprint method . . . 20
  - 4.1.2 Polynomial method . . . 21
  - 4.1.3 RASTAR method . . . 21
- 4.2 Results of indicators on the simulation . . . 22
  - 4.2.1 Fingerprint results . . . 22
  - 4.2.2 Polynomial method results . . . 22
  - 4.2.3 RASTAR method results . . . 23

5 Experimental validation 27
- 5.1 Test set-up . . . 27
- 5.2 Experiment description . . . 28
- 5.3 Results and discussion . . . 28
- 5.4 Comparison to numerical . . . 31

6 Conclusions 33

7 Recommendations & Future work 34

A FRF 37

B Conference Proceeding 37

1 Introduction

A fundamental part of maintenance technology is monitoring the structural integrity of the system. By doing so, the remaining life of a component in operating conditions can be accurately predicted. Researchers and companies recognise the importance of maintenance by investing in research in better diagnostic tools.
In recent years, interest surrounding extension of life of components has increased. In the past, components where replaced upon failure, which resulted in much unexpected downtime. This improved when components were replaced on a timed interval, for instance after every month. The downside to this scheme is that it does not consider the actual operating hours of the system in that time. If this knowledge would be included, even further improvement would be made to the maintenance scheme. However, this approach still means that the full lifetime of the component might not be reached, and replacement would not have been necessary yet. The solution lays in monitoring the structural health of the system and applying a dynamic maintenance strategy based on collected data. Such dynamic maintenance strategies present schemes that suggest component replacement or repair based on its expected remaining lifetime. This will decrease downtime and overall maintenance costs. To adequately set up such a scheme, the condition of the component needs to be monitored. *Structural Health Monitoring* (SHM) focuses on detection of unhealthy dynamic behaviour as damage occurs and propagates in the structure.
There are currently many different methods available to perform SHM. The challenge is finding a method that can do this in operating conditions. Some current methods need components to be isolated from the system and tested in a more sterile laboratory environment. Other methods utilise sensors that can measure during operating conditions and can be attached to the component in the design phase. When such contact sensors are not applicable, there are various non-contact methods available. With the ever increasing capabilities of these measurement techniques, more potential and robust diagnostic tools can be developed.
In this study, a diagnostic tool is developed to assess the dynamic behaviour of a vibrating beam. The beam is clamped at one end and subjected to an excitation force at the free end. This simple cantilever system represents a component in operating condition. When damage is applied to the system, the dynamic behaviour changes. This difference caused by the damage is sought after with the diagnostic method developed in this study. SHM applications require a non-destructive diagnostic tool to assess the structural health of the system. The *Continuous Scanning LDV* method is a very fast, non-destructive and non-contact measurement method. The output spectra of this method are of interest for the development of a novel diagnostic tool that can be used for SHM.

1.1 Goal of the study

Dynamics based maintenance is highly interesting for maintenance in the industry, who are constantly looking for new and better diagnostic tools. The method presented in this paper is mainly aimed at cantilever structures such as turbine blades for power generation but could easily be extended to a much wider application field.
The goal of this study is to develop a diagnostic method based on scanning laser vibrometry. This is achieved by performing the following sub tasks:

- The literature is studied on current measurement techniques and damage detection methods.
- The beam is modelled in the finite element method to assess the dynamic behaviour and response to damage.
- A strain analysis is done to reveal the sensitivity of the system to damage.
- Multiple indicators are defined and compared to find the most robust and sensitive method.
- Experiments are conducted for the validation of the method.

The result is a novel approach based on a continuously scanning non-contact device to determine if a structure undergoes stiffness degradation with respect to a known condition. This research

did not aim at identifying the location of the damage, but instead aimed at quickly resolving the health of the structure.

1.2 Outline of the study

The study is approached as follows. Section 2 of the paper will review the most relevant measurement techniques to carry out diagnostics. The section explains the difference between the contact and non-contact techniques when applied to SHM. Next, the theory behind the *Continuous Scanning Laser Doppler Vibrometry* (CSLDV) methods is explained and the techniques that apply this to the detection of structural degradation are presented.
In Section 3, a numerical study is undertaken to examine the effect on the dynamic behaviour as a result of the structural degradation. A simple model is made in ANSYS and the CSLDV output signal is simulated using Matlab. Several damage types and severities are applied and their impact on the dynamic behaviour is assessed. A strain analysis is done to further assess the change in dynamic behaviour by the applied damage. Robustness of the spectral analysis is achieved by studying the strain energy field and to observe its changes depending on the excitation frequency. The novelty of this research with respect to the past literature is the focus on the spectral sidebands of the CSLDV output signal, which carry both spatial and temporal information on the state of the structure. The condition can be derived directly from the spectra, without resolving the deflection shape, as is commonly done in past research. The model is kept two dimensional, which severely limits the amount of spatial information that can be measured. This is a fundamental case study in which the behaviour is limited but predictable.
Section 4 presents the results of the simulations. The results are subjected to multiple damage indicators in pursuit of the most robust and sensitive indicator. The indicator yielding the most satisfying results is applied to several damage cases to assess its performance. Noise is added to the simulated LDV output signal to further study the response and robustness of the selected damage indicator.
The simulation of the final damage indicator is validated with an experimental analysis in Section 5. The results of the experiments are compared to the simulation, where only the transverse damage type is applied as described in the modelling phase.
The study finalises in Section 6 with conclusions and future plans regarding the results are listed in Section 7. In the appendix, a conference proceeding presenting part of the numerical study is displayed.

2 Background

In this section, past work in the field of structural health monitoring is reported. There are many detection techniques and processing methods to determine damage. First some common measurement techniques are summarised, both contact and non-contact techniques. Then the theory behind the CSLDV method used in this study will be further explained. A more in-depth look is taken at the processing methods to detect damage with the CSLDV technique. Finally the fundamental studies used for this thesis are stated and the implications for the present study are summarised.

2.1 Detection techniques

SHM is used to detect changes in the system that are the result of damage over time. The damage detection methods that are considered for this application are non-destructive and based on vibration analysis. Damage detection methods can be categorised as either contact or non-contact.

2.1.1 Contact methods

When a damage detection method uses sensors that are attached to the structure in question they are considered contact methods. Most common sensors to be used for SHM are piezoelectric strain gauges and accelerometers, as Chopra reviewed in [1]. Strains/displacements generate a voltage in the strain gauge which can be measured. This can then be related to the structural integrity of the system at the sensor locations. Accelerometers are similar to strain gauges but measure the accelerations instead of the strains. Another contact technique that is gaining interest in the field of sensing is the use of fibre optics, where reflecting light gives information on the strain on the component the fibre is attached to. Multiple sensors and multiple types of sensors are commonly applied to one component to monitor the condition.
These sensors are used in various methods to detect damage. In the research of Johnson et al. [2] a sensor array was used to describe dynamic transmissibility features as indicators of structural damage. Both accelerometers and strain gauges where used, which lead to the recommendation for future work to research the trade-off between high strain but low accelerations at the root of a cantilever beam and vice versa at the tip.
A common application field of dynamic maintenance are wind turbine blades. This is the subject of the research of Sierra-Pérez et al. [3], who used fibre optics to detect damage and compared the results to conventional strain gauge methods. It was found that the number of sensors that were needed to adequately perform SHM was too high to be viable. However, it was claimed that fibre optics could become much more applicable in composites if they are embedded in the product during the production process.
Abry et al. [4] proposed a method to detect damage in composites by measuring a change in electrical resistance. Copper electrodes were placed at both ends of the beam and a current is send through. The study showed that very low damage levels could be detected.
Contact methods are sometimes not viable under operating conditions, because they require expensive and/or complicated electronics for transferring the data. Other reasons that the techniques are not applicable are too extreme temperatures in operating conditions or rotation of components. Also, determining the location of the sensors is model based, an FEA needs to be conducted to find the proper sensor placement. Non-contact, non-destructive damage detection methods might offer alternatives.

2.1.2 Non-contact methods

Many remote sensing methods have been researched, a selection is presented here, keeping in mind their application in SHM. A widely used and researched method is Digital Image Correlation (DIC). DIC compares multiple digital photographs of a vibrating structure. The pixels in the high resolution photographs are tracked and after post-processing, a strain-field can be composed. The high contrast and light intensity levels that are required for this technique can be reached in a laboratory environment if adequate lighting is used. In the study, McCormick and Lord

[5] presented that the texture of most structures is enough for the tracking software to pick up. However, Avril et al. [6] found that in applications outside the lab, surface treatment is often needed to allow for consistent tracking. This considerably lowers the in situ SHM measurement capabilities of this technique.
Detecting damage in composite beams can be done using a thermal camera. When a delamination between two plies occurs, the areas rub together and cause heat due to friction. This heat is conducted to the outer surface and can be captured with a thermal optic or infra-red camera. Mian et al. [7] used infra-red surface imaging to detect such a delamination. This thermal effect can also be induced by the detection method itself, using sound wave pulses to vibrate crack surfaces, causing them to locally heat up. Currently, this technique is most commonly used for composite materials. The technique can also be applied to metals, but mostly in destructive test environments and near-yield strength tests, as explained by Pastor et al. [8]. The high amounts of stress initiates dislocations and their movement causes the resulting heat. Small and gradual damage progression through metals does not produce such heat and is therefore not a viable measurement method.
The advances made in laser technology allowed for an increase in research of non-contact damage detection methods using laser light. Speckle interferometry is a technique that uses multiple laser beams as well as a camera to extract phase information of a vibrating structure. Jacquot [9] summarises the basic principles behind the widely researched Speckle interferometry technique. The patterns that arise from the interfering laser beams on the rough surface, together with video, yields information on the response of the system to excitation. Hertwig et al. [10] have taken this technique and implemented it for SHM purposes; it can be used for both a pristine and damage case to find differences due to structural degradation. The speckle interferometry technique requires a very expansive and precise set-up. A closely related technique, Holography, uses roughly the same set-up. It is capable of acquiring comprehensive data from the system, as De la Torre et al. [11] reviewed. Holography differs from Speckle interferometry in that it requires the reconstruction of its 3D complex amplitude [9]. The sterile environment and expansive set-up make these measurement techniques inappropriate for assessing structural health in operating conditions.
Another Non-contact measurement technique that uses laser light is *Laser Doppler Vibrometry* (LDV). Castellini et al. [12] present the applications of LDV methods, including SHM. In its core, LDV uses a laser beam, which is reflected off a surface, also called backscatter, and collected by a detector. When this is measured (scanned) over time, not only spatial information is obtained, as is the case in Speckle interferometry, but also temporal information. This technique is commonly referred to as Scanning LDV (SLDV). SLDV can be done at discrete points (Stepped SLDV) or with sweeping mirrors, (Continuous SLDV). Both are viable techniques to be used in SHM. However, Stepped SLDV needs several seconds of measuring per discrete measurement point, which is time and data intensive. *Continuous SLDV* (CSLDV), scans a line or area over the specimen for several seconds to obtain the information, which makes it a much faster technique. It obtains information from virtually thousands of points in one measurement. The theory behind the CSLDV technique and its application to SHM are explained more in-depth in the section below.

2.2 Theory on scanning laser vibrometry (CSLDV)

As stated above, the *Continuous Scanning Laser Doppler Vibrometry* (CSLDV) method can obtain spatial and temporal information of a vibrating system in a matter of seconds. This makes it a viable technique for rapid damage detection. In this section, the theory behind the method is elaborated upon.

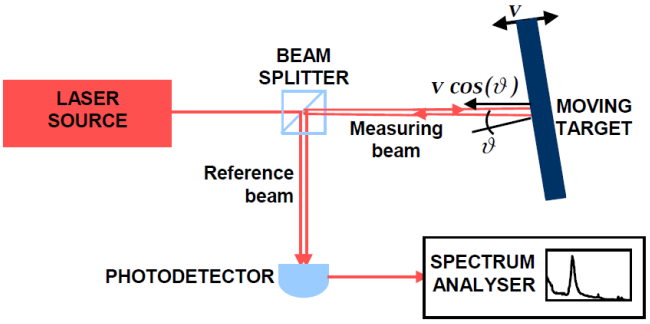

Figure 1: Basic LDV set-up [13]

In Figure 1 the basic LDV set-up is schematically drawn. The laser source is stationary and emits a monochromatic laser beam with a high intensity. This is passed through a beam splitter to create a reference beam and a measuring beam. The measuring beam hits the target and is backscattered to the detector, then it is compared to the reference beam. When the measured surface is vibrating, and the laser source and detector are stationary, the relative motion causes a frequency shift of the light in the laser beam. The shift is related to the relative velocity of the system, also known as the Doppler effect. This is why the monochromatic light from the laser beam is ideal for measurements using the Doppler phenomenon. This frequency shift can be picked up by the detector, allowing for calculation of the moving velocity of the target surface.
Scanning LDV uses this basic LDV set-up combined with scanning mirrors. The mirrors point the laser beam at different points on a grid. The target is then excited and information is obtained during a few seconds. When the data is collected, the laser is pointed to the next point of the grid by rotating the mirrors. The target is excited again and the information is collected. This continues for every point on the measurement grid, once the data from all points is collected, it is post-processed and the *Operational Deflection Shapes* (ODS) can be derived. The ODS is the shape in which the specimen is vibrating. As stated before, this approach is very time consuming and very data intensive, since a comprehensive analysis needs a very dense measurement grid.
The scanning mirrors that move the laser beam over the measurements grid can also be used to move continuously, while the measurement is taking place. This is referred to as Continuous SLDV. The main advantage over SLDV is that it scans a virtually infinite number of points in the same time it takes SLDV to scan just one point. The CSLDV method can scan a line sinusoidally, or scan in a pattern over an area.
Some previous work by Stanbridge ad Ewins [14] explored this technique in the form of modal testing, where the advantages of CSLDV method are described. The CSLDV method output is a time signal, which can be modulated to a frequency spectrum. It was shown that this spectrum contains information on the modal parameters of the system. This work is elaborated upon by Martarelli [13], where the basic principles and working of the CSLDV method are described. The theory on simulating the CSLDV method and applying the modulations as used in the present thesis is obtained from this Ph.D. Thesis.
The potential to use CSLDV for damage detection in vibrating structures is clear and has been researched. Most research depend on reconstructing the ODS from the CSLDV output signal, as done by Chen et al. [15]. After obtaining the ODS in polynomial form using the demodulation method, the curvature of the polynomial ODS was used to identify abnormalities from the pristine case. More research found that CSLDV could be used to detect cracks in a cantilever beam. A transverse crack of more than half the thickness of the beam was identified by Khan et al. [16], by looking at the frequency response. Discontinuities in the mode shape where found, but only under very specific loading and heavy damage conditions.
The behaviour of a steel plate was also researched in pursuit of novel damage detection methods. The damage was simulated by adding a magnet to the plate and analysing its effect on the dynamic response, using different excitation locations. In the research, Di Maio et al. [17] used continuous area scanning as well as grid measurements, and compared them to numerical results. The damage was measured by taking the Mean Square Error (MSE), as well as a more sensitive adaptation

of it, between the pristine and damaged ODS. This research concludes with a need for a better, more sensitive damage definition. This is sought after in another research by Di Maio [18], that strictly covers numerical simulations. This paper introduces the use of the frequency spectrum, characteristic to the CSLDV method. A beam is simulated with different damage severities. The frequency response of the beam is simulated and the spectrum analysed. The paper finds that solely using the spectrum would be enough for health monitoring.

2.3 Implications for the present work

The findings summarised above form the basis for the present work. A damage indicator should be found, based solely on the output spectrum of the CSLDV method, without the need of extracting the ODS. Past research has focused on not only detecting damage but also locating it and/or quantifying the severity. In this thesis, just the detection of damage would be enough. The problem set in [18] is reduced to two dimensions. This makes it a worst-case scenario in terms of spatial information that can be acquired, but also makes the behaviour controllable and predictable.

3 Numerical Study

In this Section, the numerical aspects of the study are described. First, a finite element model is made to simulate the behaviour of the system specified. The damage implementation and boundary conditions are described here. Next, a strain analysis is performed in which the behaviour of the model is further assessed. Some deflection shapes and strain distributions are analysed and compared and a identification strategy is defined. Finally the data from the simulations is collected and the output of the CSLDV method is simulated.

3.1 Finite element model

A numerical model is made in the *Finite Element Method* (FEM) using ANSYS Mechanical APDL 16.2. For this study, a prismatic, cantilever beam is defined. The beam is clamped at one end and subjected to an excitation force in y-direction at the free end. The conventional material properties of aluminium are used, as listed in Table 1. The beam dimensions are given in Table 2.

Table 1: Beam properties

Material property	Value
Young's Modulus	69 MPa
Density	2700 kg/m^3
Poisson's Ratio	0.334
Damping Ratio	0.004

Table 2: Beam Dimensions

Designation	Length
Length (l) x-direction	400 mm
Thickness (t) y-direction	10 mm
Width (w) z-direction	40 mm

3.1.1 Specification on element configuration

The simulation of the beam will be kept to a strictly two-dimensional approach. The idea is to keep the structure as simple as possible to get a very predictable response. Another advantage is that this way of modelling allows for application of a wide variety of damage types, by altering the stiffness properties of the elements that are considered damaged. This approach allows for many crack path designs, such as transverse crack, delamination or interlaminar crack paths.
Three element configuration are described here. A number of tools and analyses are used to review their performance in the FEA. The models are compared using the same material properties, dimensions and number of elements. First a static analysis is done, comparing the tip deflection of the model to the analytic solution described by equation 1. The force (F) at the tip dictates the maximum deflection (δ).

$$\delta = \frac{Fl^3}{3EI} \tag{1}$$

Analytically, with a force of 100 N this yields a deflection of 9.275 mm. The maximum deflection per element configuration is presented in Table 4. A modal analysis is done to obtain the eigen-frequencies of the system, which can be compared to the analytical solution. The analytical values for the i^{th} eigen-frequency are calculated with equation 2. The dimensions and properties of the beam as described above are used, the constants for a cantilever beam are: $A_1 = 1.875$, $A_2 = 4.694$ and $A_3 = 7.854$.

$$\omega_i = A_i^2 \cdot \sqrt{\frac{EI}{ml^3}} \tag{2}$$

The minimum number of elements to be used in the simulations is based on a sensitivity analysis. To set a baseline mesh, the sensitivity analysis is undertaken for *PLANE182* elements. These elements are meant for 2D modelling of solid structures, it is an element with four nodes and two *Degrees Of Freedom* (DOF). Five meshes are defined with increasing refinement, see Table 3. A modal simulation is done for each mesh, a finer mesh will obviously perform better, but the computation time also increases. The mesh is considered '*good enough*' when the improvement stagnates in relation to the growth of the mesh size.

Table 3: Model mesh size

Iteration	1	2	3	4	5
Mesh(txl)	5x50	10x100	20x200	30x300	40x400

The first three eigen-frequencies from the simulations are compared to the analytical values. The analytical values for the i^{th} eigen-frequency are calculated with equation 2. Using the dimensions and properties of the beam described above. The error of the simulation is then calculated using equation 3. The results are plotted in Figure 2. The error of the first three eigen-frequencies obtained by the different models of the other element type with the same number of elements are displayed in Table 4.

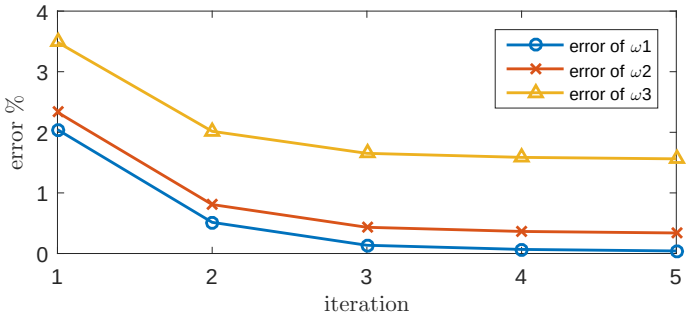

Figure 2: Mesh sensitivity analysis

$$\text{error} = \frac{|\omega_{sim} - \omega_{ana}|}{\omega_{ana}} \cdot 100\% \tag{3}$$

From Figure 2, it can be concluded that iteration 3, or 20x200 elements, is enough as the increase in performance is very minimal from that point on.
Two element types are evaluated, *PLANE182* and *SHELL181*. *PLANE182* was briefly described above. *SHELL181* is a four node, 3D element with six DOF, if membrane stiffness is included. If not, the element only has 3 DOF (no rotations). Membrane stiffness is used when the main deflection shape is out of plane. For this application, in plane bending of the elements, only membrane stiffness is used. Both full and reduced (red.) integration are considered, since multiple elements through the thickness of the beam are chosen.

Table 4: Comparison of deflections and resonances of different elements

	PLANE182	SHELL181 (Full)	SHELL181 (Red.)	Analytical
Max. δ (m)	0.00916	0.00914	0.00916	0.00928
Error ω1 (%)	0.136	0.002	0.002	-
Error ω2 (%)	0.433	0.290	0.023	-
Error ω3 (%)	1.653	0.727	0.726	-

The values from Table 4 show that the textitSHELL181 element with reduced integration is the best choice, since it is closest to the analytical solution. Investigating the deflection shapes revealed a problem with this element. The elements started to behave problematic in higher frequency range, the nodal displacements became very unstable. The ODS of one of the problematic frequencies was plotted for all three element configurations. An example frequency of 8500 Hz is shown in Figure 3 for all three element configurations.

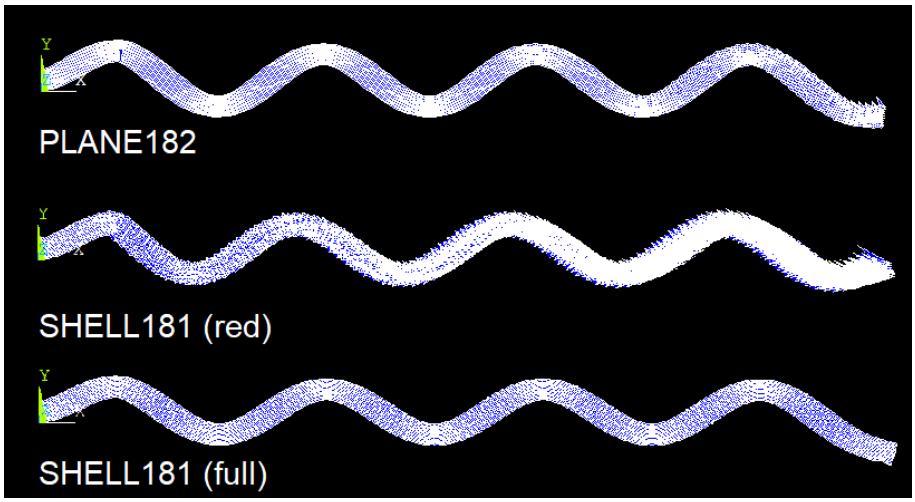

Figure 3: Deflection shape from ANSYS for three element configurations

In Figure 3, the elements at the tip on the right-hand side start to become very unstable for both the *PLANE182* and the *SHELL181* with reduced integration. The elements deform in a non-realistic way, as can be seen by the fuzzy shape. Re-running the simulation with more elements to make it stable did not solve the problem. *SHELL181* with full integration performed second best in Table 4 and behaves more stable at these frequencies. This is the selected element configuration for the simulations in this work.

3.1.2 Damage typology

As said before, damage is applied to the model by altering the stiffness properties of the elements. This can be done in a number of different ways:

- Deleting damaged elements
- Reducing thickness of damaged elements
- Replacing damaged SHELL elements with spring elements
- Assigning different material properties to damaged elements

For stability in obtaining convergence in the simulation of the beams response, continuity in the beam is of major importance. This is why completely deleting the elements is not advisable. Reducing the thickness of the elements, especially in a two-dimensional model is motivated by [19] and [20]. Replacing the *SHELL* elements with springs is common practice but adds modelling complexity when crack paths throughout the beam would be modelled. Assigning different material properties such as lower Young's modulus is less common and could easily alter the dynamic behaviour of the model too much or in unexpected ways. As a reference, the results found in [21] are used as guidance. In the study, two cuts are made, at around 40- and 80% of the beams length, the maximum depth of the cracks is about 30% of the beams thickness. Numerical and experimental analysis in the study show a frequency shift of 1.5% for the second bending mode.
As explained before, multiple different crack paths can be modelled. The current study is limited to two distinct damage types. A transverse crack, or saw cut, and a delamination, or longitudinal cut. A delamination is not expected to occur in an aluminium beam, this is implemented as a theoretical damage case only. Both damage types will be modelled and analysed in three severities: 2 elements (10% thickness), 5 elements (25% thickness) and 10 elements (50% thickness). The transverse crack originates from the bottom and is applied at 0.04 m from the root, which is at 10% of the beams length. The delamination will grow toward the free end from 0.04 m and is located at 2.5 mm below the neutral axis. The damage designations for future reference are defined in Table 5.

Table 5: Damage designations

Length		Transverse	Longitudinal
2 elements	1 mm	D10T	D10L
5 elements	2.5 mm	D25T	D25L
10 elements	5 mm	D50T	D50L

3.1.3 Final model configuration

For this study, 4000 *SHELL181* elements with membrane stiffness only and full integration will be used. The first column of 21 nodes will be locked in x-, y- and z-direction. A force of 100 N in positive y-direction is placed on the node in the bottom row of the 199^{th} (out of 200) column. The damage is applied to the model by reducing the elements that represent the damage in thickness in z-direction by 90%. All nodes are locked in z-direction to make it a strictly 2D problem. The material properties of aluminium are used.
In Figure 4, the final ANSYS model configuration is displayed. The arrows on the left-hand side of the white beam visualise the clamping. The red arrow on the right visualises the force. The expanded part of the beam displays the possible damage typologies. Red for the transverse damage, green for the delamination and purple for possible interlaminar damage cracks (not implemented in this study).

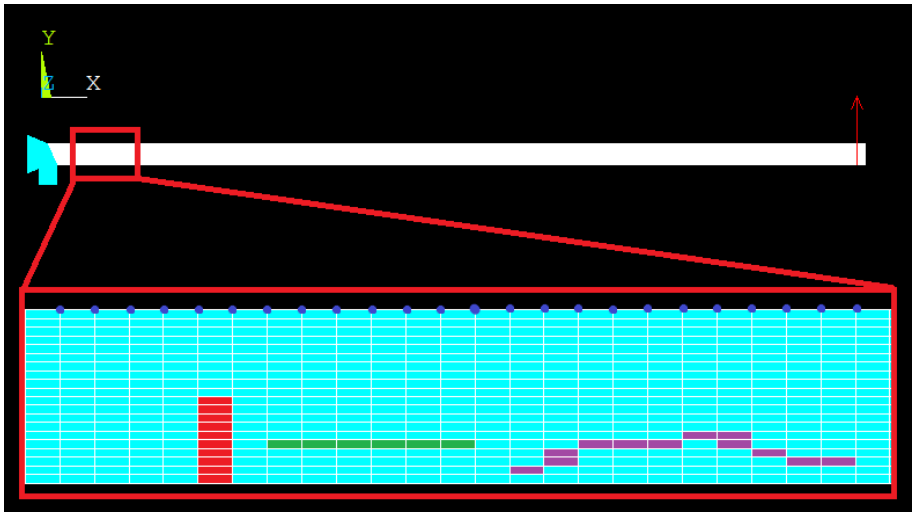

Figure 4: Final ANSYS model configuration

3.2 Strain Analysis

Following the numerical modelling, a strain analysis is performed on the simulations. The *Operational Deflection Shapes* (ODSs) are observed for both the eigen-frequencies and the anti-resonances. This is done at the fixed pristine eigen-frequencies. If the corresponding eigen-frequency of the damaged case are compared instead, the ODS would be almost exactly the same. The strain energy distributions over the ODSs are compared to distinguish which frequencies would be most sensitive to the applied damage.

3.2.1 ODS comparison between pristine and damage case

The simulation results heavily depend on the ODS, the shape induced by the excitation force and frequency. At the (anti-) resonances, a characteristic shape is expected. The damaged elements, which are reduced in thickness, exhibit a local stress concentration. This changes the strain distribution over the entire beam, resulting in a slight change in the ODS at that fixed frequency. This should then be picked up by the CSLDV method and after post-processing result in a positive indication for damage. The ODS is extracted from the model by taking the y-component of

displacement of the top row of nodes. These nodes are marked with blue dots in Figure 4. The ODSs of the first six eigen-frequencies are shown for the pristine and damaged condition in Figure 5 and for the first six anti-resonances in Figure 6.

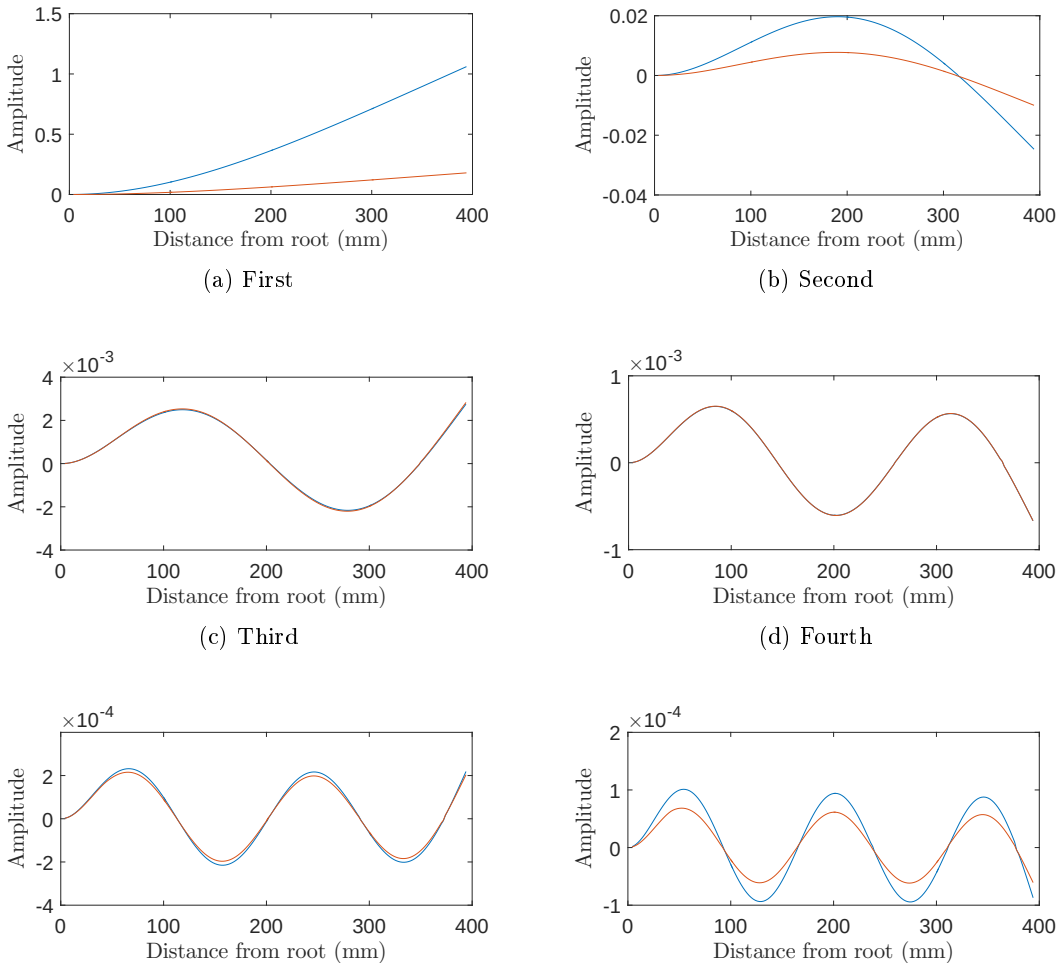

(a) First (b) Second

(c) Third (d) Fourth

(e) Fifth (f) Sixth

Figure 5: ODS of first 6 eigen-frequencies for pristine (blue) and damaged (red) case

The blue lines represent the pristine cases, the red lines the damaged cases. As can be seen, the change in ODS is very minor for a fairly large damage case (D50T), especially for the anti-resonances. All pristine shapes are as expected, the maximum amplitude of the ODS becomes lower for every eigen-frequency. The amplitude of the anti-resonances are overall lower than the eigen-frequencies. A sensitivity analysis is done to further investigate the strain behaviour at these frequencies.

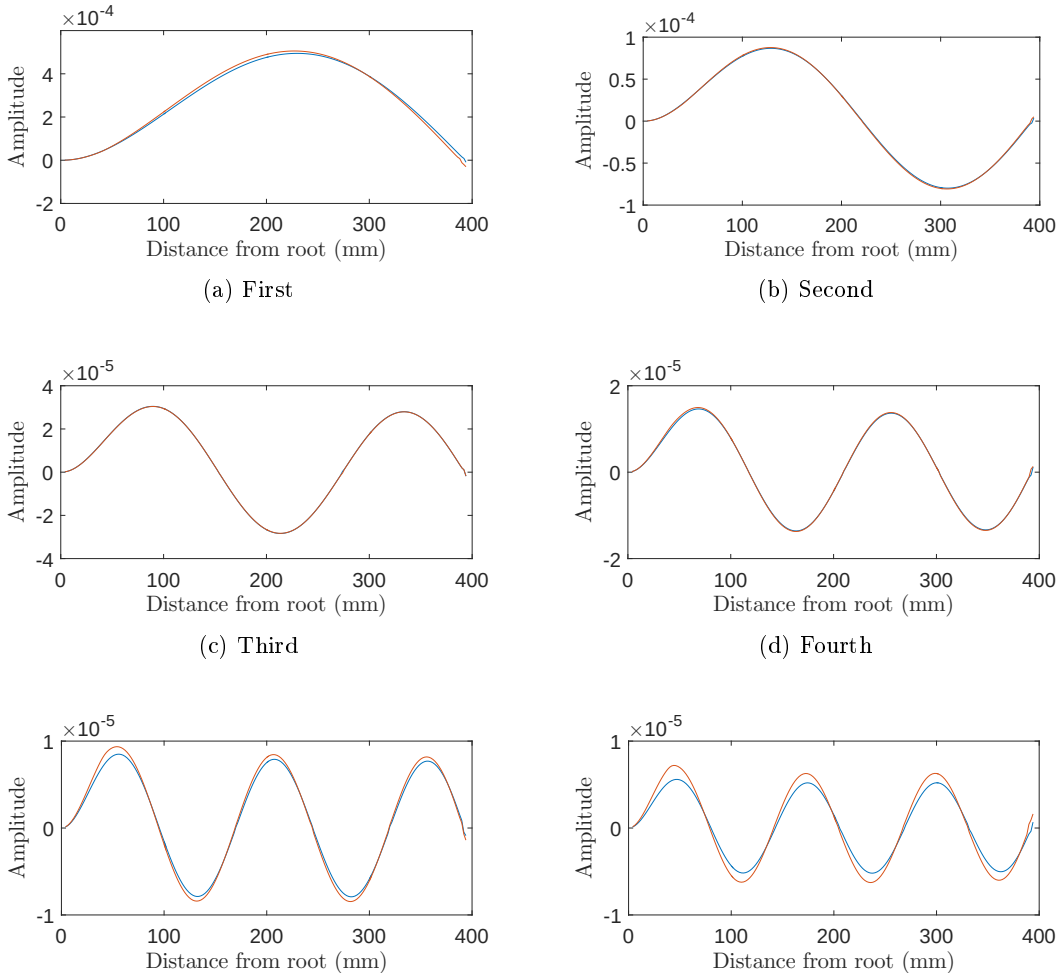

(a) First (b) Second

(c) Third (d) Fourth

(e) Fifth (f) Sixth

Figure 6: ODS of first 6 anti-resonances for pristine (blue) and damaged (red) case

3.2.2 Sensitivity of dynamic behaviour to the damage

The sensitivity of the model is shown per eigen-frequency in Table 6. Here, for three damage severities, the eigen-frequencies and phase are listed. The phase shift is measured at the pristine eigen-frequency.

Table 6: Response to damage severity

	Frequency (Hz)				Phase shift at ω^P (deg)			
Eigen	Pris	D10T	D25T	D50T	Pris	D10T	D25T	D50T
ω_1	51	51	50	50	-79	-134	-164	-170
ω_2	319	318	317	316	-94	-117	-145	-158
ω_3	889	889	888	887	-92	-97	-107	-117
ω_4	1731	1731	1731	1731	-96	-94	-92	-91
ω_5	2837	2837	2835	2833	-94	-97	-105	-115
ω_6	4196	4193	4184	4178	-96	-108	-131	-142
ω_7	5794	5785	5766	5750	-100	-120	-148	-157
ω_8	7616	7602	7571	7546	-104	-127	-154	-163

What can immediately be seen is that the fourth eigen-frequency does not seem to be effected by the damage at all. This also seems to be the case when the ODS is observed in Figure 5d. To see

why this is the case, the strain energy distribution along the beam is plotted in Figure 7 for various eigen-frequencies. Isolating the fourth eigen-frequency in Figure 8, it can be seen that the strain energy is very low at the damage location, 40 mm from the root. When the ODS is inspected, it becomes clear that this is an inflection point of the ODS. This means that very little stress is put on the damaged elements. This behaviour is compared to the second eigen-frequency, which does show a lot of sensitivity in Table 6. As can be seen from Figure 9, the strain energy at the damage location is much higher in this case. This means that the change in dynamic behaviour as a result of damage is frequency dependent. In search of a sensitive damage indicator, an identification strategy is set up to assess what frequencies show most sensitivity to the damage.

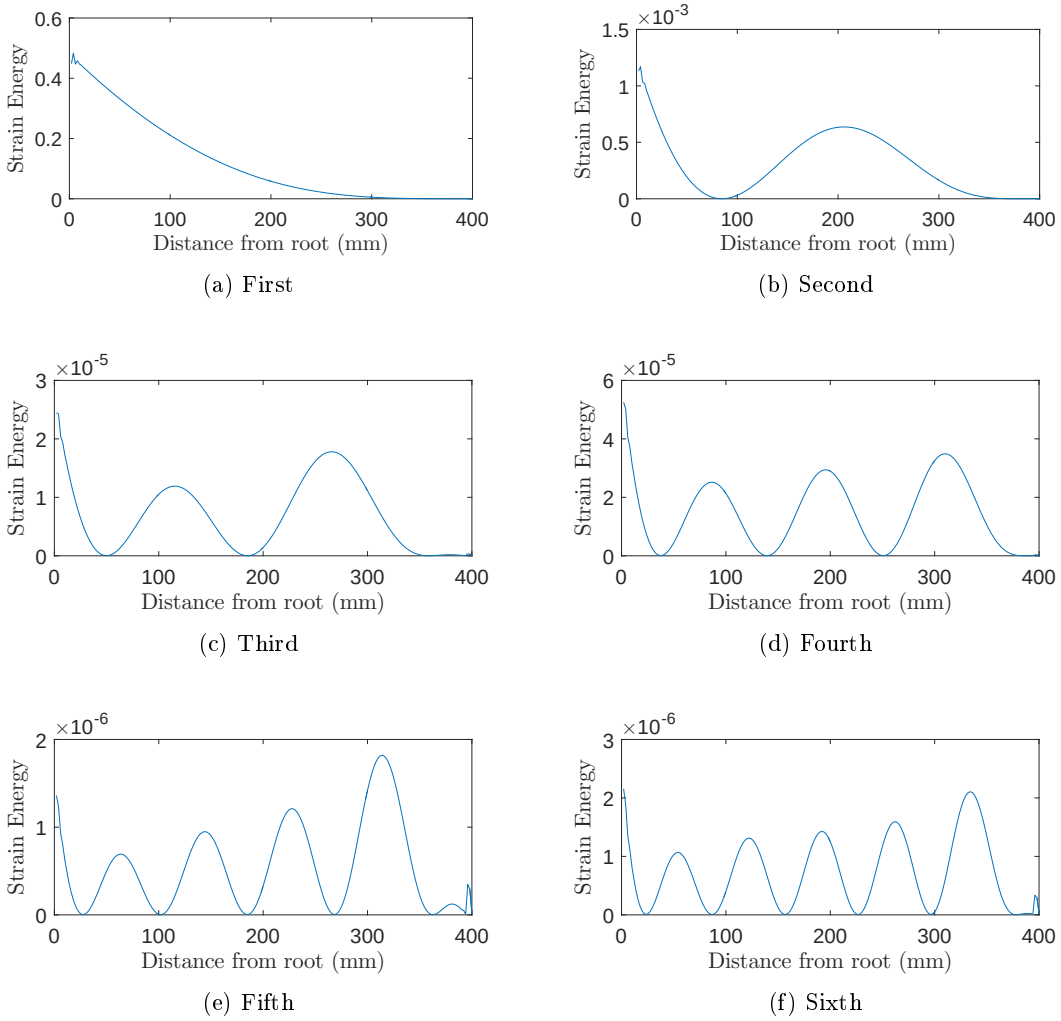

(a) First (b) Second

(c) Third (d) Fourth

(e) Fifth (f) Sixth

Figure 7: Strain energy of first 6 eigen-frequencies

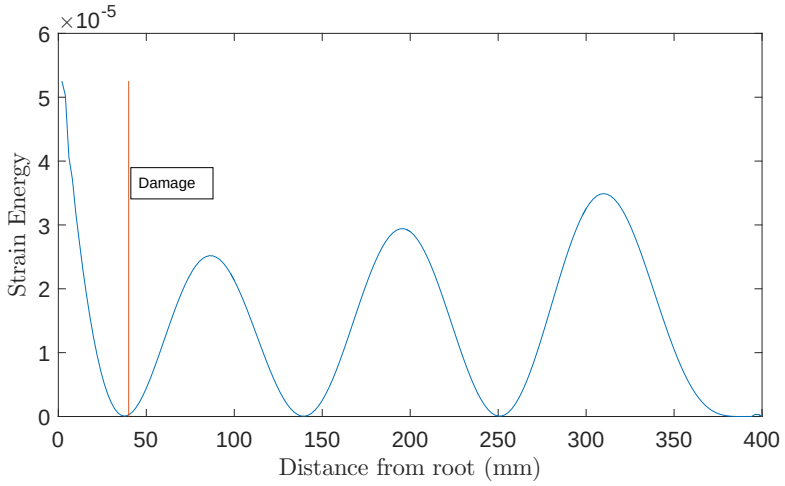

Figure 8: Strain energy at damage location

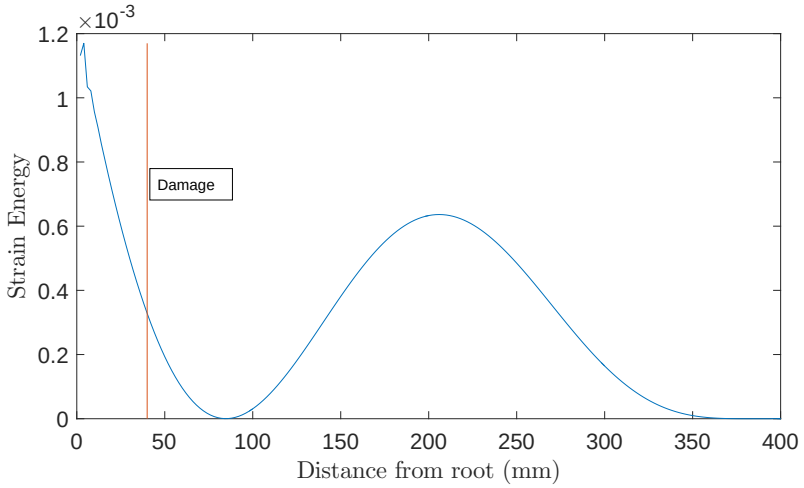

Figure 9: Strain energy at damage location

3.2.3 Identification strategy

The eigen-frequencies and anti-resonances are compared to each other and a table of the strain energy at the damage location is made, see Table 7. The values at the damage location are listed for all resonances and anti-resonances. It appears that for higher frequencies, the anti-resonance would be more sensitive to the applied damage than the resonances. These anti-resonances show higher values than its surrounding eigen-frequencies. This is portrayed by the percentage in the fifth column that displays the percentage increase or decrease (-) of strain energy between the resonance and the following anti-resonance. The sixth column shows this difference between the anti-resonance and its following resonance.

Table 7: Strain energy at damage location for resonance and anti-resonance

Res. (n)	Strain Energy (10^{-6})	Anti Res. (n)	Strain Energy(10^{-6})	Δ SE n:n	Δ SE n+1:n
1	448540				
		1	49.6970	-99.98 %	-87.87 %
2	409.62				
		2	3.9423	-99.04 %	236.92 %
3	1.1701				
		3	0.0095	-99.18 %	-96.16 %
4	0.2477				
		4	0.8234	232.42 %	213.08 %
5	0.2630				
		5	2.1810	729.28 %	171.37 %
6	0.8037				
		6	3.1822	295.94 %	61.44 %
7	1.9711				
		7	3.5857	81.91 %	28.79 %
8	2.7842				

The strain energy of the fifth and sixth eigen-frequency and fifth anti-resonance are plotted in Figure 10b. Interestingly, the strain energy peaks are higher for the anti-resonances. Based on the findings from Figure 8, a very low strain energy at damage yields a low sensitivity of the dynamic behaviour to the damage. The anti-resonances seem to be interesting frequencies to investigate further. While past literature like [15] only focusses on the eigen-frequencies. The anti-resonance shape seems to imply an additional constraint to the cantilever structure, which in turn could be the cause of the higher strain energy results.

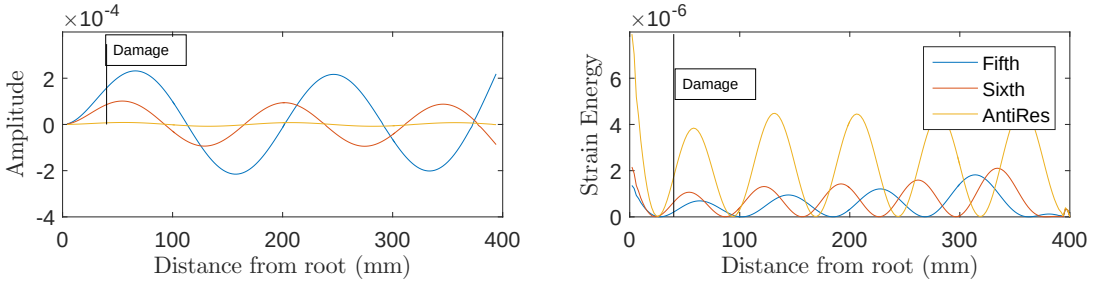

(a) ODS

(b) Strain energy distribution

Figure 10: ODS and strain energy of 5th and 6th eigen-frequency and 5th anti-resonance

3.3 Simulation of output spectrum using CSLDV method

CSLDV measures velocity information along the complete length of the vibrating beam. To obtain this from the numerical model, the y-displacements of all nodes in the top row of the model are extracted for all frequency responses. These nodes are marked with blue dots in Figure 4. The selected frequency range is 1 to 9000 Hz with a frequency step of 1 Hz. Next, the mathematical model is applied to construct the time signal that the CSLDV method would give. These time signals are then put through a Fourier analysis and the output spectra are generated.

3.3.1 Damage severity based on Frequency Response Function

The data is analysed using Matlab. Both amplitude and phase information of the y-displacement of the top row of nodes is acquired. First, the *Frequency Response Function* (FRF) is made for the tip of the beam. This is done in Figure 11 for the Pristine case (blue line) and the D50T damage case (red line).

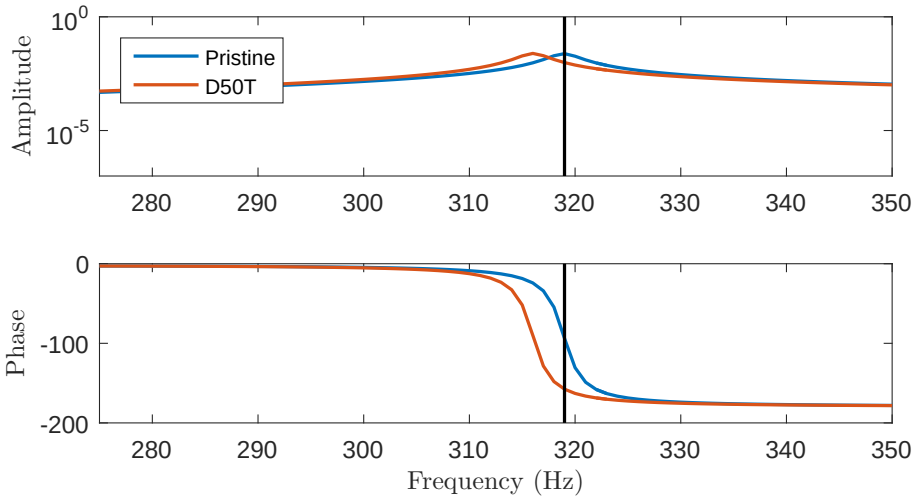

Figure 11: Frequency Response Function of P & D50T (zoomed)

In Figure 11 a close look is taken at the second eigen-frequency of the FRF, the full FRF of the tip of the beam can be found in Appendix A. Equation 2 presented the calculation on the analytical eigen-frequencies. EI/L is an equivalent measure for stiffness k, so an easier way of calculating the first eigen-frequency is shown in equation 4.

$$\omega_{(1)} = \sqrt{\frac{k}{m}} \tag{4}$$

According to equation 4, the eigen-frequency is proportional to k/m, where k is stiffness and m is mass. The eigen-frequency obviously shifts when damage is introduced to the system. The damage applied to the structure reduces the stiffness in the beam, as described by Ostachowicz and Krawczuk [22]. This property is also commonly used to assess the sensitivity of a system to damage. As said before, the damage is modelled in three severities. For each severity, the frequency shift is calculated in the same manner as equation 3. However, for a given structural damping, the phase angle of a damaged structure shows much larger deviation from the pristine condition than the frequency shift. To show this, both the frequency shift, Figure 12, and the difference in phase angle at the pristine eigen-frequency, Figure 13, are plotted for each damage severity of the transverse damage case. The shifts observed in the Figures have been presented before in Table 6 in the previous Section.

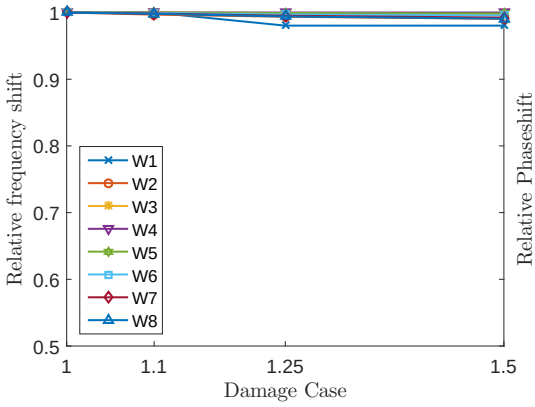

Figure 12: Frequency shift

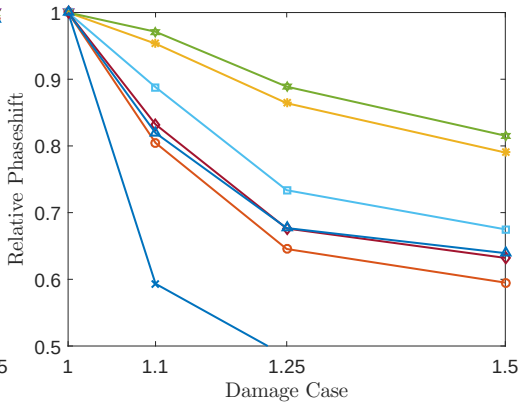

Figure 13: Phase shift

As can be seen in the Figures, the phase angle shows a high sensitivity to the applied damage. This is heavily dependent on the damping, in this case a constant structural damping coefficient of 0.004.

3.3.2 Operational Deflection Shape definition

The next phase in simulating the output spectrum is extracting the Operational Deflection Shapes (ODSs) from the model for all frequencies. This is done by performing a harmonic analysis and evaluating the y-displacement of all the top row nodes for all frequencies. These values are described in amplitude and phase, with which the ODSs are constructed.
The x-coordinate of the beam is normalised to be -1 at the root and 1 at the tip, making 0 the middle and the a normalised beam length of 2, using equation 5. This is done to allow for simulation of the continuous sinusoidal line-scan.

$$X_{norm} = \text{Scale} \cdot X + \text{Offset} \tag{5}$$

Where:

$$\text{Scale} = \frac{1}{\frac{1}{2} \cdot (\max(x) - \min x))} \qquad \text{Offset} = -1 \tag{6}$$

The normalised length is used as the new x-coordinate of the ODS. Now a *polyfit*-function is used in Matlab to obtain the polynomial coefficients of the ODS shape. This function approximates the shape with a polynomial like in equation 7.

$$f = A_0 + A_1 x + A_2 x^2 + A_3 x^3 + ... \tag{7}$$

The amount of polynomial coefficients needed to adequately describe the ODS is dependent on the frequency, since a higher frequency vibration shape is more complex and thus requires more polynomial coefficients. The minimum number needed is calculated by the Modal Assurance Criterion (MAC), equation 8, which relates the approximate shape to the real shape [23]. To get an idea of the necessary amount of coefficients, the MAC value necessary to describe the eigen-frequencies is evaluated. The number of coefficients is increased as long as the MAC value is below 0.999. The results are shown in Table 8.

$$\text{MAC} = \frac{(\Phi_a \cdot \Phi_r^T)^2}{\Phi_a \cdot \Phi_a^T \cdot \Phi_r \cdot \Phi_r^T} \tag{8}$$

Where Φ_a is the approximate polynomial by the *polyfit*-function and Φ_r is the ODS from the model.

Table 8: Minimal Nr. of Coefficients

eigen-freq.	1	2	3	4	5	6	7	8
Nr. of coeff.	2	4	5	8	9	10	13	14

In the following Sections, 15 polynomial coefficients are used for all frequencies. This means that higher order terms will be close to zero for lower frequencies.

3.3.3 CSLDV output signal using ODS

Now the shapes of all 9000 frequencies are approximated by polynomial functions, the time signal can be simulated. As stated before, the CSLDV method uses a continuous sinusoidal line-scan that scans the vibrating beam. The CSLDV measures the velocity of the vibration, this can be written as equation 9.

$$v = \sum_{n=0}^{p} A_n x^n \cos(\omega t) \tag{9}$$

Where the first part is the polynomial described in equation 7, ω is the vibration frequency and p is the number of coefficients. The equation is obtained from [13], the ODS is assumed real. Since the x-component is normalised, equation 10 can be used for the scan-line.

$$x(t) = \cos(\Omega t) \tag{10}$$

Where Ω is the scan rate of the laser. When this is plugged in as the x-component of the polynomial in equation 9, the function for the time signal becomes:

$$v(t) = \sum_{n=0}^{p} A_n \cos^n(\Omega t) \cos(\omega t) \tag{11}$$

This is the final equation for simulating the time signal obtained by the CSLDV. For the simulation, a sampling rate of 20 kHz and a test time 10 seconds per frequency is used. Obeying equation 12 for minimal sample frequency (f_s) at 9000 Hz excitation frequency (f_n).

$$f_s \geq 2f_n \tag{12}$$

The result is a time signal whose envelope resembles the vibration shape of, in this case, the second eigen-frequency. This is shown in Figure 14. Since the plot is very dense, a zoom is shown in Figure 15. In this Figure, the composition of the time signal can be seen more clearly.

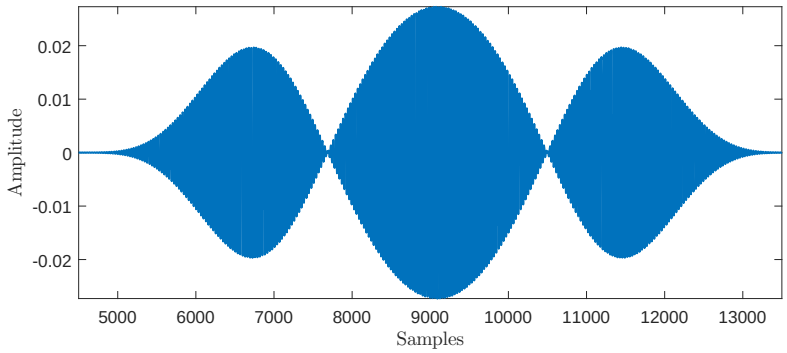

Figure 14: Portion of time signal of second eigen-frequency

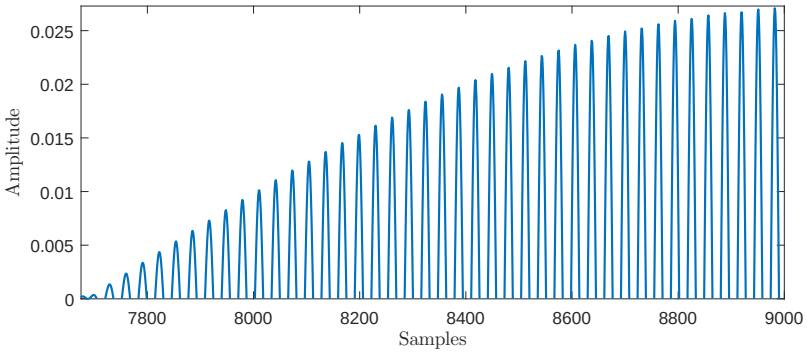

Figure 15: Scan rate in time signal

The time signals processed by *Fast Fourier Transform* (FFT). As can be seen in equation 11 above, the time signal is composed of various frequencies. FFT translates the time signal into the frequencies which make up the signal. Discrete FFT (dFFT) does this only at a discretised frequency interval. The dFFT is discretised at the excitation frequency (ω) and subsequently at interval of the scan rate (Ω). This yields a symmetric spectrum around the excitation (or middle) amplitude with equally spaced sidebands around it, as seen in Figure 16. The number of one sided sidebands, seen on the x-axis, equals the amount of polynomial coefficients. The magnitude of these sidebands carry spatial information of the ODS. The mathematical relation between the sidebands and the polynomial coefficients, and thus the ODS, are explained in [14].

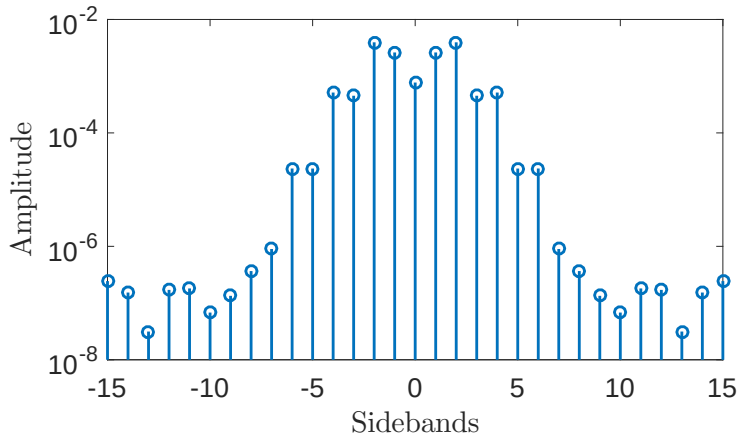

Figure 16: dFFT at 2nd eigen-frequency

Since the amplitude of the sidebands carry this information, the distribution of these sideband amplitudes can be considered characteristic for a specific system at a fixed excitation frequency. When damage is introduced to the system, its dynamic response changes, and thus, the spectrum changes. This can be seen in Figure 17. The blue stems show the pristine case and the damaged case is displayed by the red stems, at the pristine second eigen-frequency.

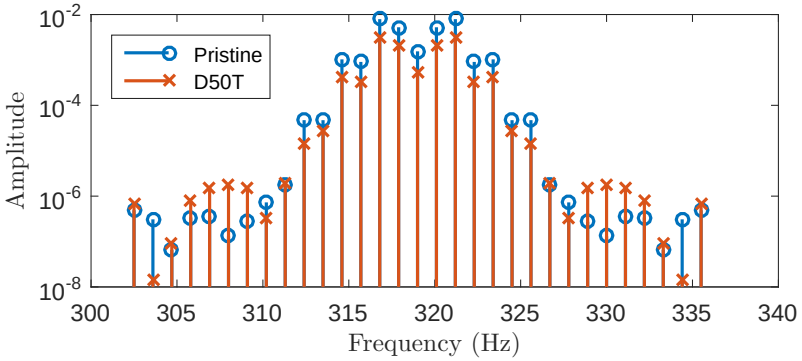

Figure 17: dFFT at pristine 2nd eigen-frequency (Pris and D50T)

The stems representing the damaged case are clearly lower at the first few sidebands than the pristine stems. This is as expected, because the amplitude in the FRF at the pristine eigen-frequency is higher for pristine case than for the damaged case, as seen in Figure 11. If measured at the pristine eigen-frequency, the excitation amplitude is no longer at a peak if the beam is damaged, explaining the lower overall amplitude of the damaged sidebands. In the higher order sidebands more change in the distribution is visible. As said before however, these higher order terms are near zero and hold little meaning for the ODS at these excitation frequencies. What is clear, is that the distribution of the sideband amplitudes has changed from its characteristic one, it has not just shifted down.
The insight that the spectrum changes from its characteristic shape when damage is introduced to the system can be exploited for SHM purposes. This behaviour was already seen in earlier work [20]. The next step is developing a damage indicator that computes this change in sideband amplitude distribution. This is elaborated upon in Section 4. The same methodology of extracting the spectrum is done on the time signals obtained by the experimental analysis in Section 5, which is done to verify the numerical analysis.

4 Damage indicator definitions

In this Section, the results from the numerical study are displayed and analysed to define different damage indicators. Then the results of the defined damage indicators are compared. The most robust and sensitive indicator is tested on multiple damage types and severities. Finally, white noise is added to the frequency spectrum for the selected damage indicator.

4.1 Development of damage indicators

In Section 3 the methodology towards the numerical approach was explained. It was determined that the dFFT of the time signals would be used to define a damage indicator. The indicator is required to distinguish whether the spectral sideband amplitudes are not just shifted in overall amplitude, but individually present different behaviour. As was already seen in the higher order sidebands in Figure 17. In the real world, the sidebands will be affected by noise, which means a robust damage indicator is needed that can adequately assess the distribution of sideband amplitudes of the spectrum despite the noise. In the following subsections, noise will be disregarded to first find an indicator that can adequately compare the spectra, keeping in mind the overall lower amplitude of the damaged case at pristine eigen-frequency with respect to the pristine case.

4.1.1 Fingerprint method

Comparing the pristine and damaged spectra directly by subtraction does not compute a relevant indication of the damage. It is therefore important to normalise the sideband amplitudes of the pristine and damaged case to make them comparable. A change in distribution of the sideband amplitudes must be found regardless of the excitation amplitude. This condition is used to define a damage indicator where all sideband amplitudes are normalised to the middle, or excitation amplitude. In this way, the vertical shift in the spectrum is avoided, the middle amplitudes will normalise to 1 in both cases. The result is a *fingerprint* of the shape of the spectrum for that frequency. If change is observed in this fingerprint, damage must have occurred. This is mathematically expressed in equation 13. Where the fingerprint amplitude ($\mathrm{FPA}_i(\omega)$) of the i^{th} sideband at excitation frequency ω is calculated by dividing the i^{th} sideband amplitude (SBA_i) by the middle amplitude.

$$\mathrm{FPA}_i(\omega) = \mathrm{SBA}_i(\omega + \Omega \cdot i)/\mathrm{SBA}(\omega) \tag{13}$$

By doing this for i from 0 to 15 for the respective cases, all amplitudes become a factor of the middle amplitude. Now the shapes can be compared, this is done in Figure 18 for the second eigen-frequency. The blue line represents the pristine case and the red line the damaged case. As expected, the higher order sidebands immediately show the different behaviour. This is, again, less relevant due to the low absolute value of the amplitudes and the little meaning these hold for the deflection shape. Figure 19 shows that also for the first few sidebands the fingerprint is different.

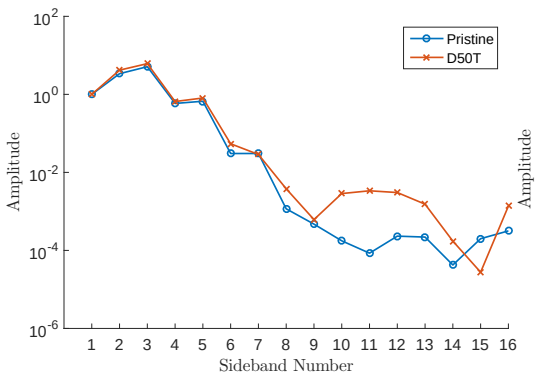

Figure 18: Fingerprint method

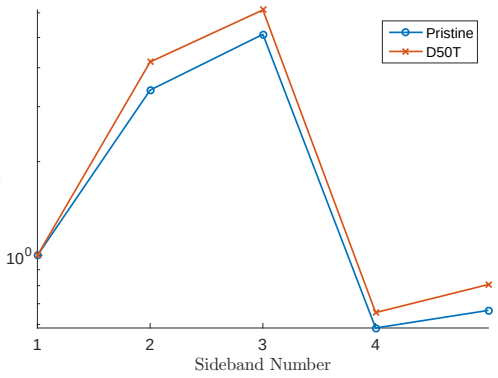

Figure 19: Fingerprint zoom

As can be seen in the Figures, the method seems to work for the second eigen-frequency. Turning this result in a scalar value indicator would make the method more readable and comparable when

multiple frequencies are assessed. Detecting damage from Figure 18 can be done, but assigning a scalar value would be preferable. One way to quantify the plot in Figure 18 is to take the *mean square error* (MSE) between the two cases. The MSE is expressed in equation 14, with p as the number of sidebands.

$$\mathrm{MSE}(\omega) = \frac{1}{p}\sum_{i=1}^{p}(\mathrm{FPA}_i^{\mathrm{Pris}}(\omega) - \mathrm{FPA}_i^{\mathrm{D50T}}(\omega))^2 \tag{14}$$

4.1.2 Polynomial method

Another method that is explored is based on the relation between the spectral sideband amplitudes and the polynomial coefficients of the wave shape of the ODS. Spatial differentiation of the polynomial function results in a function related to the strain. When damage is introduced to the system the strain distribution changes. This also causes a change in the ODS at that frequency, which is a polynomial function. This knowledge is used to define some damage indicators based on the sideband amplitudes. The first sideband corresponds to the linear term, the second to the quadratic, and so on. This can be recognised in the indicator descriptions in equations 15, 16, 17 and 18:

$$\mathrm{PM}_1 = \sum_{i=1}^{p}\mathrm{SBA}_{\mathrm{Pris}}(\omega \pm \Omega i)^i - \mathrm{SBA}_{\mathrm{D50T}}(\omega \pm \Omega i)^i \tag{15}$$

$$\mathrm{PM}_2 = \sum_{i=1}^{p}\mathrm{SBA}_{\mathrm{Pris}}(\omega \pm \Omega i)\cdot i^{(p-i)} - \mathrm{SBA}_{\mathrm{D50T}}(\omega \pm \Omega i)\cdot i^{(p-i)} \tag{16}$$

$$\mathrm{PM}_3 = \sum_{i=1}^{p}\mathrm{SBA}_{\mathrm{Pris}}(\omega \pm \Omega i)\cdot i^{i-1} - \mathrm{SBA}_{\mathrm{D50T}}(\omega \pm \Omega i)\cdot i^{i-1} \tag{17}$$

$$\mathrm{PM}_4 = \sum_{i=1}^{p}(\mathrm{SBA}_{\mathrm{Pris}}(\omega \pm \Omega i)\cdot i^{i} - \mathrm{SBA}_{\mathrm{D50T}}(\omega \pm \Omega i)\cdot i^{i})\cdot \omega \tag{18}$$

Where ω is the excitation frequency and Ω is the scan rate, p is the number of polynomial coefficients. Since the first few sidebands hold most information on the shape and the strain, the indicators are also tried including less than all 15 sidebands. These are four different indicators based on the same approach of using the relation between sideband amplitudes and the polynomial coefficients. Different factors per sideband are used to find the most sensitive indicator to the difference in strain behaviour.

4.1.3 RASTAR method

Another method called the RASTAR method is devised. This method evolved from the fingerprint method. RASTAR stands for Relative Amplitude of the Sidebands to the Total Amplitude Reference. Where the fingerprint method based its normalisation on only one (the middle) sideband, this method makes use of all sidebands. To normalise the amplitudes of both cases, first, the amplitude of all sidebands in the spectrum is summed, referred to as the *total amplitude*. The individual sideband amplitude is calculated as a percentage of the total amplitude; every sideband is assigned a percentage value of its relative contribution to the total amplitude. This is expressed in equation 19. By doing so for the pristine and damage cases, the relative contribution percentages per sideband can be compared. The damage indicator for that frequency is acquired by summing all differences per relative sideband. A lesson learned from the polynomial sideband method is that this RASTAR method can be applied for any number of sidebands chosen. As said before, at lower frequencies, most information is in the first few sidebands, so only applying the method for these sidebands would not change the sensitivity much. It would change for higher frequencies, since more sidebands are needed to describe the shape.

$$\epsilon(\omega) = \sum_{j=1}^{n}\left(\frac{SBA_P(\omega \pm \Omega j)}{\sum_{i=1}^{n} SBA_P(\omega \pm \Omega i)}\cdot 100\% - \frac{SBA_D(\omega \pm \Omega j)}{\sum_{k=1}^{n} SBA_D(\omega \pm \Omega k)}\cdot 100\%\right) \tag{19}$$

4.2 Results of indicators on the simulation

4.2.1 Fingerprint results

A scalar value damage indicator is defined, so it can now be applied over the full frequency range. The result can be seen in Figure 20, MSE from equation 13 is displayed on the y-axis. The graph shows a few very high spikes (10^7) which make it an inconsistent and unreadable graph.

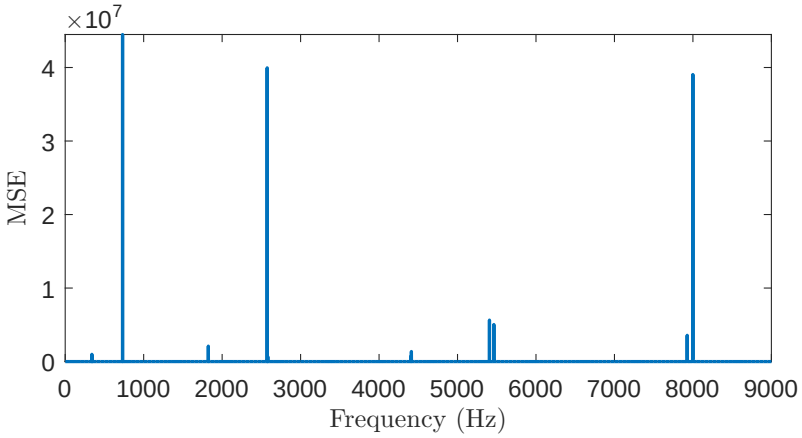

Figure 20: Mean Square Error for all frequencies

The reason for these spikes is investigated. The first local maximum, at 731 Hz, in Figure 20 is selected and the spectrum is viewed in Figure 21a. The middle amplitude is very low in relation to the first sideband for the pristine case. This is also true for the damaged case, however considering the log scale y-axis, the difference between these two cases is around a factor of 100. The impact that this has on the MSE is more easily identified by looking at the resulting fingerprint in Figure 21b. It can be concluded that this large difference in the middle amplitude, which is used for normalisation, results in unusually large Mean Square Errors. Since this behaviour does not occur consistently and in varying levels throughout the frequency range, the method is deemed unstable.

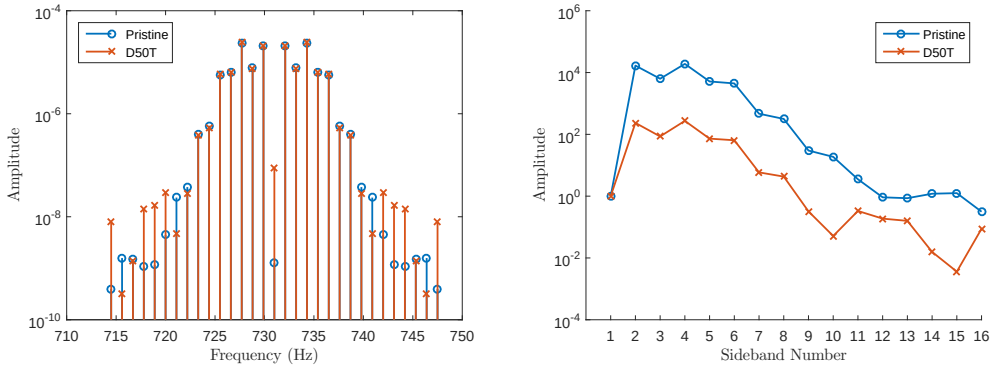

(a) FFT

(b) Fingerprint

Figure 21: Problem case Mean square error

4.2.2 Polynomial method results

In the polynomial method, multiple possible indicators are mentioned to calculate the reaction to the damage. The main difference with the fingerprint analysis is that here, the sideband amplitudes are not normalised. This makes the magnitude of the resulting damage indicator heavily dependent on the frequency, at the resonance the magnitude will be higher. All approaches have similar results in terms of shape, all need to be plotted on a log scale for comparison.

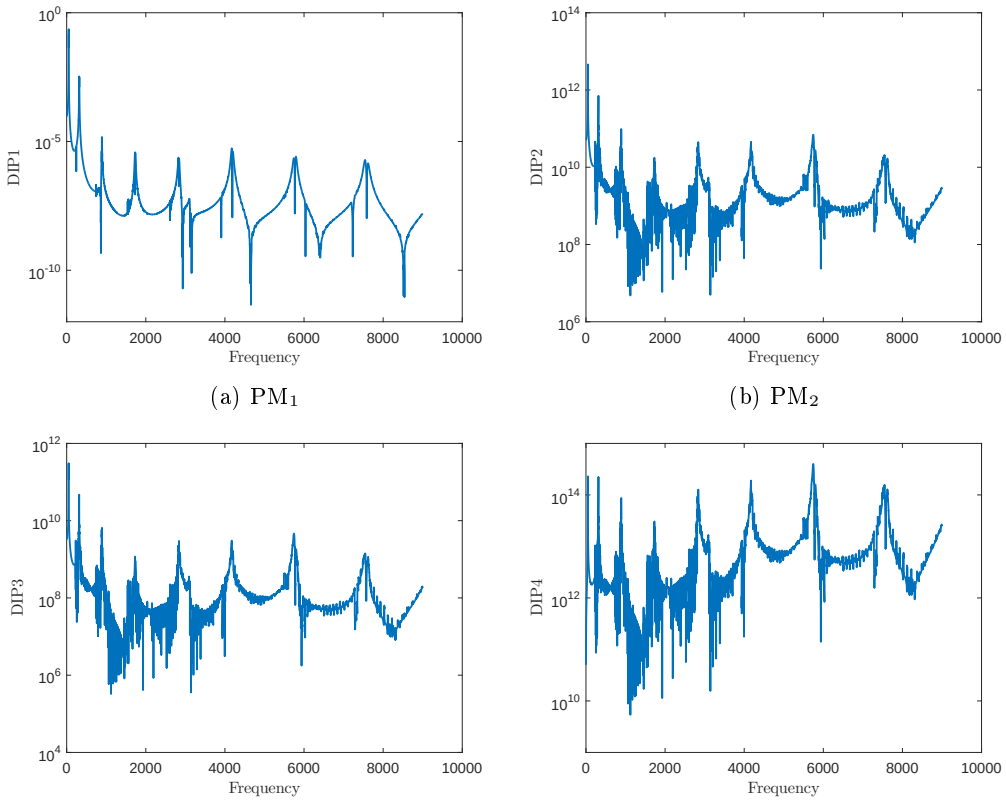

(a) PM_1 (b) PM_2

(c) PM_3 (d) PM_4

Figure 22: Polynomial method results from equations 15, 16, 17 & 18

One large difference between the four is the magnitude itself, ranging from 10^{-10} in Figure 22a to 10^{14} in Figure 22d. As is clear from the logarithmic y-scale, the method is very volatile, the magnitude of the damage indicator shifts too much over the frequency range for it to be a robust damage indicator.

4.2.3 RASTAR method results

In this method, all the sidebands in the spectrum are used to normalise the relative sideband amplitude to a percentage of the summation. As explained above, the amount of sidebands that are included in the calculation can be varied at will. The effect of changing the amount of included sidebands can be seen in Figure 23, all three are the pristine case compared to the D50T damage case. This method seems to behave more consistently. The indicator shows peak values at the anti-resonances. As expected, the lower frequencies show little change from using more sidebands, since the higher order terms do not hold much meaning for these frequencies. However, even for the higher frequencies, the lower amount of sidebands taken into account seem to result in a more sensitive indicator at the anti-resonances, but less at all other frequencies.

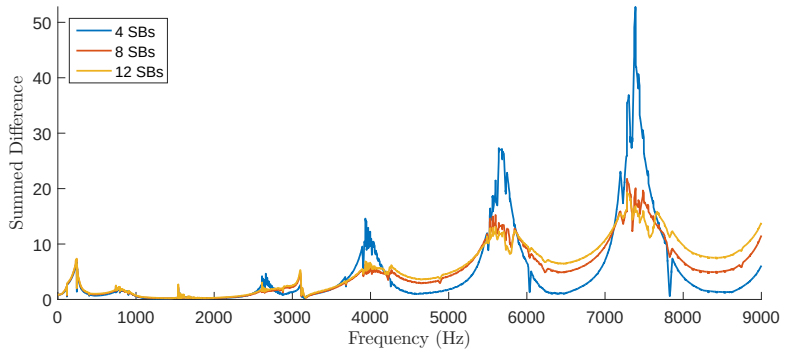

Figure 23: RASTAR method for 4,8 & 12 sidebands

The method yields fairly consistent values over the frequency range. Figure 23 shows the 50% damage case, which is a relatively excessive damage. To check the sensitivity the lower damage severities are also plotted in Figure 24. The indicator behaves as expected, a gradual increase in damage results in a gradual increase in damage indicator. The overall shape remains similar.

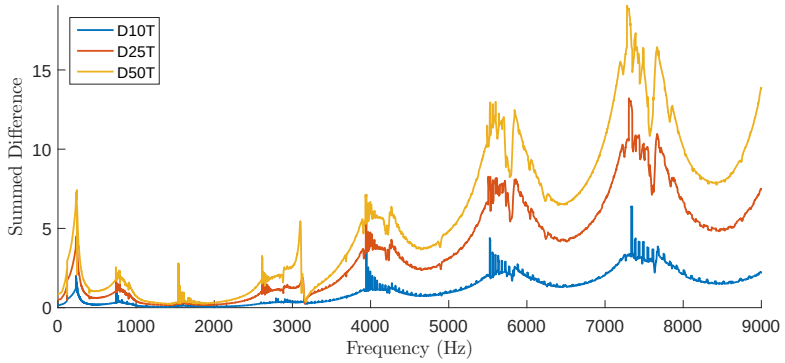

Figure 24: RASTAR method for three damage severities

The damage indicator should only indicate damage if there is any. Therefore, the pristine simulation is ran once more, this time with the excitation force halved. This should not change the dynamic behaviour of the sidebands, but only cause a vertical shift in overall amplitude. This case is then compared to the original pristine case and the D10T damage case, the smallest damage case. The result is shown in Figure 25. As can be seen, the blue line, which represents the damage indicator for the pristine case compared to the pristine case at low force, is non-existent in relation to the damaged case. The method works regardless of the input force. So this shows that just a vertical shift in the spectrum does not result in an indication for damage.

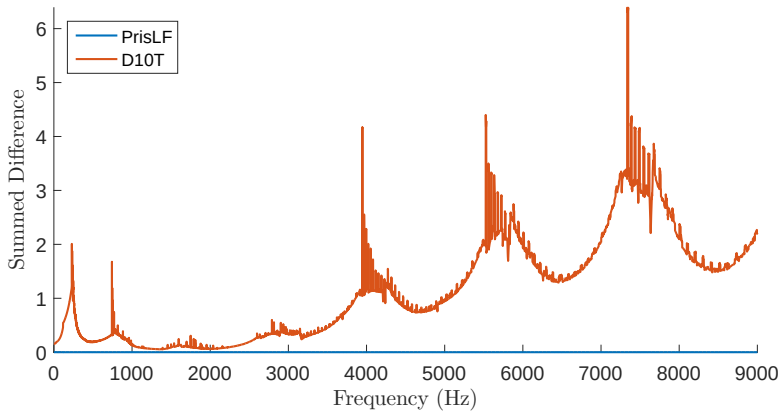

Figure 25: Pristine at Low Force comparison

Longitudinal damage

As mentioned in Section 3.1, longitudinal damage, or a delamination, is also modelled and simulated. The RASTAR method is also used to calculate the indicator for this damage type. The three severities are compared and plotted in Figure 26. As can be seen in the Figure, the behaviour is as expected, increasing damage results in increasing indicator. When compared to the transverse damage in Figure 24, the indicator is less sensitive to the longitudinal damage. As said before, this is not a damage type that is expected to occur in an aluminium beam, this is just for proof of concept purposes. The indicator should not solely detect transverse cracks.

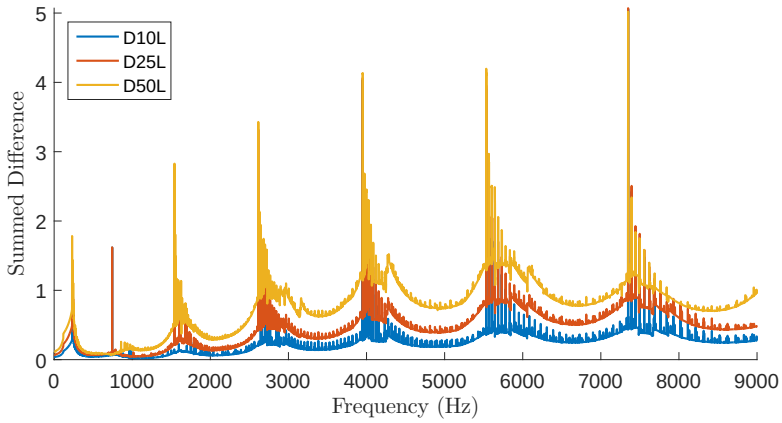

Figure 26: Three severities of longitudinal damage

Introduction of random noise

Numerically the generated time signal is perfect without loss of data. The damage indicator should however be robust enough to generate a higher damage indicator value than the noise floor in a more realistic environment. When the overall amplitude is low in the simulation, the criterion still works if there is no noise. This would be different in the real world where no perfect signal is generated. White noise is added to the sideband amplitudes of every spectrum. A random number between 0 and 1 is generated and multiplied with (10^{-8}). This random value is then added to all sideband amplitudes over the full frequency range. This does not produce realistic noise, since the power level is uniform over the frequency range in this simulation, but gives a good indication on how robust the method is. The indicator for a damaged case should always yield a higher value than the benchmark. The benchmark is the pristine case with random noise, compared to a pristine case with different random noise.

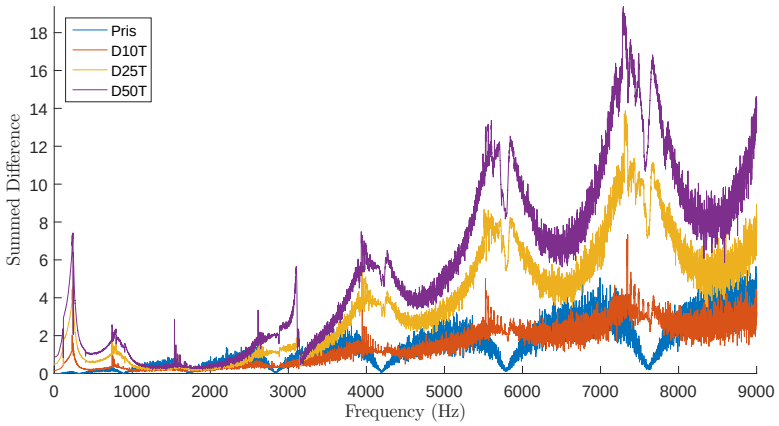

Figure 27: Damage indicator for transverse damage cases with random noise

In addition to all damage severities, the benchmark case is plotted (blue line). A distinctive behaviour is seen by the benchmark case. Some frequencies show a near-zero indicator value, these are the eigen-frequencies, where the signal-to-noise ratio is very high and is therefore less effected by the noise. It is clear from Figure 27 that in the higher frequencies ($>$ 3000 Hz), the 10% damage case can result in a lower indicator value than the benchmark. This is not the case in the lower frequencies, which can be seen better in Figure 28. Here, a clear distinction can be made between all damage severities and the benchmark, despite the noise. This means that selection of frequencies to test is important for damage detection.

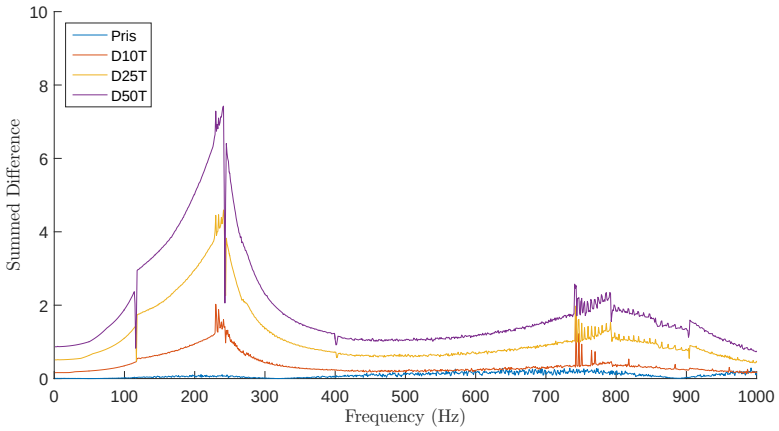

Figure 28: Zoom of damage indicator for the 4 cases up to 1000 Hz

5 Experimental validation

The results obtained in the numerical study are validated by experimental analysis. The experiments are conducted with the knowledge that the result will differ from the numerical model. The general behaviour is expected to be the same, the peaks of the indicator at the anti-resonances as found in the numerical analysis are not expected to be as high, mainly because of the lower expected signal-to-noise ratio. First an overview of the test set-up is described. Then the procedure used for the experiments is explained. Finally the experimental results are discussed and compared to the numerical results.

5.1 Test set-up

For the experimental analysis, a test set-up was build. A steel L-frame was available in which the samples could be clamped. The frame was bolted to a metal plate using steel framework and bolts to fasten it down. The metal plate is fixed to a concrete block on rubber legs to damp most vibrations from the room. The specimen is an aluminium beam of 30 mm wide and 10 mm thick. The length is approximately 500 mm, but the beam is clamped to have an effective length of 400 mm. The difference in width to the simulation does not matter for the eigen-frequencies, as explained with equations 20. The beam is categorised as aluminium 6082-T6. The laser used for the experiment is the Polytec PSV-I-560. The laser is positioned sufficiently far from the rig so the mirror rotation allows for the laser to scan the entire length of the beam. As in the simulation, only the bending of the beam should be measured. Some torsional component is expected in the experiment. To minimise this, the laser is aligned with the middle of the beams width. The system will only use the x-scanning mirror, so the scan head must be as level as possible. This makes sure only the centre line of the beam is measured, which should only show bending.

$$\omega_i = A_i^2 \cdot \sqrt{\frac{EI}{ml^3}} = A_i^2 \cdot \sqrt{\frac{E\frac{bh^3}{12}}{bhl\rho l^3}} = A_i^2 \cdot \sqrt{\frac{E\frac{h^3}{12}}{hl\rho l^3}} \tag{20}$$

At the free end of the beam, a shaker is attached via a stinger and a force gauge. The force gauge is glued directly to the beam. The shaker is connected via an amplifier to the computer with the control and acquisition software. The shaker is set up to excite the beam at a horizontal angle. The computer is also connected to the laser head and controls the scanning mirrors. A picture of the experimental set-up is shown in Figure 29.

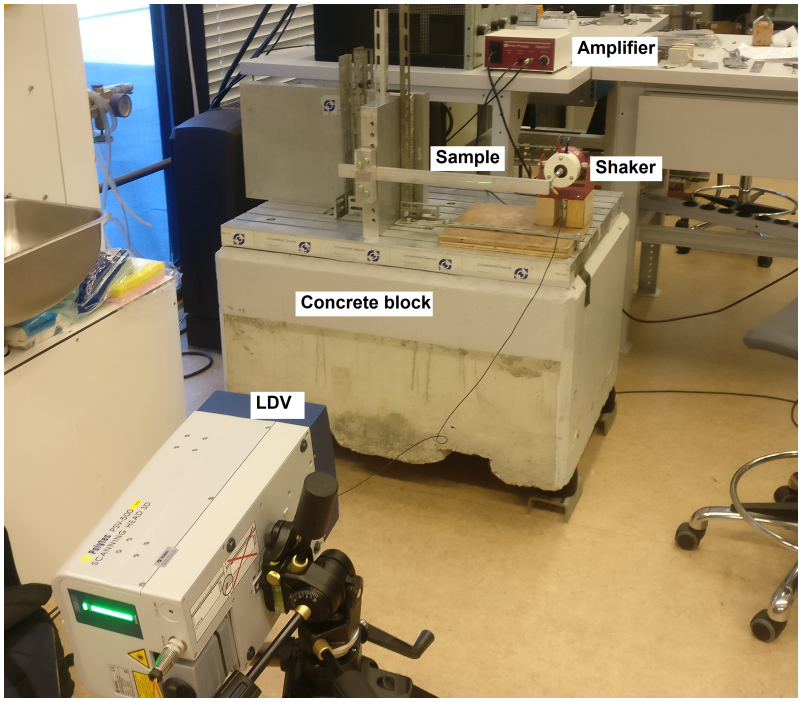

Figure 29: Experimental set-up

5.2 Experiment description

The experiments are conducted for six cases, three damage severities and two scan rates. The damage cases are: Pristine, a 1 mm by 1 mm cut at 40 mm from the root, and a 2 mm by 2.5 mm cut at 40 mm from the root. The scan rates are set at 1.1 Hz and 0.9 Hz. For all tests, the same beam is used. Conducting the experiments for the full frequency range used in the numerical analysis is not considered viable. Aluminium does not have a fatigue limit and fatigue will start to be a factor if the full range would be tested for multiple damage severities. Considering this and limited time, a frequency range is defined. The tests are done from 20 to 1000 Hz with a frequency step of 1 Hz. In this frequency range, the numerical results indicate a clear difference between the damage severities, even in the presence of noise. This is because the excitation amplitude of the beam is relatively high in this region, yielding a favourable signal-to-noise ratio. The trade-off is that in the simulation the higher frequencies result in the highest peaks in the damage indicator. In the region below 1000 Hz the settings of the laser precision, sample rate and force amplification can be kept constant and still yield good results throughout.
Before every run, the FRF of the tip of the beam is collected with the laser, up to 2000 Hz to find the eigen-frequencies and anti-resonances. Then, the test is done for the specified frequency range and the time signals are saved for every frequency. Every frequency is scanned for 10 seconds with a sample time of 9.765625E^{-5} seconds. After both scan rate tests for one damage case are done, the beam is removed from the rig and milled to the damage specification mentioned above.
The time signal is post-processed in the same manner as in the simulation, a dFFT at the specific scan rate up to 15 sidebands is performed. To reduce noise, the left- and its respective right-hand sidebands are averaged, since these should be equal. The damage indicator is calculated for all frequencies, the results are discussed in the following section.

5.3 Results and discussion

The FRF of the pristine beam is viewed in Figure 30. The first 3 eigen-frequencies and anti-resonances are marked. The FRF shows that the beam does not vibrate in pure bending motion, as expected some torsional vibration modes can be seen. These are some of the small peaks between the resonances of the bending modes.

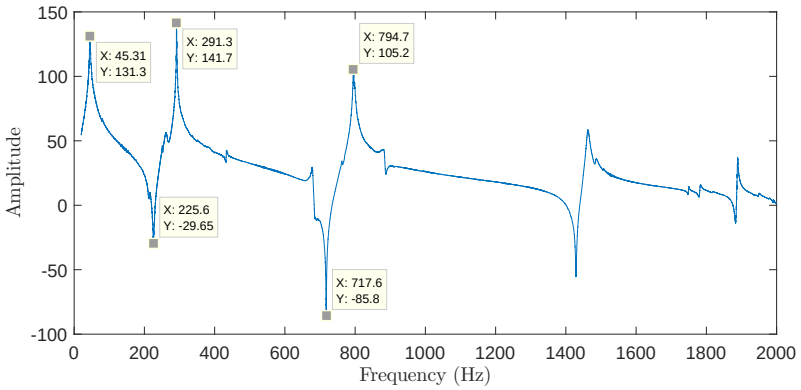

Figure 30: FRF of Pristine case

First, for the benchmark case, the pristine case of 1.1 Hz scan rate is compared to the 0.9 Hz scan rate. The result shown in Figure 31 behaves as expected. At the resonances of the beam, the signal-to-noise ratio is very high, resulting in a low damage indicator. In between the eigen-frequencies, a higher indicator value is reached due to the noise.

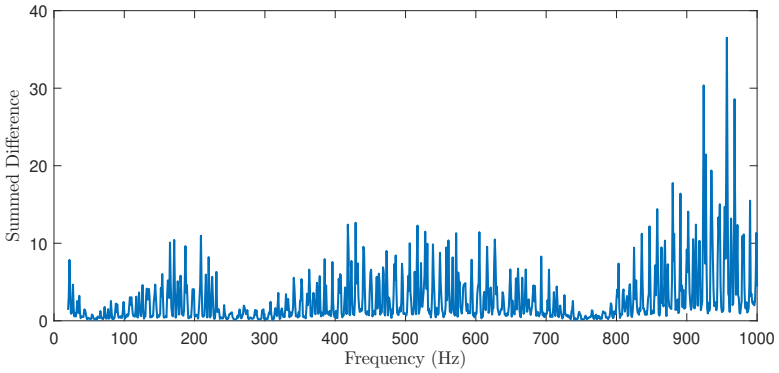

Figure 31: Unfiltered results of benchmark case

The output spectra of the pristine case at the 1.1 Hz scan rate are compared to the 1 mm damage case and the 2.5 mm damage case. This is done in the same manner as described above in the indicator definition using equation 19 for the RASTAR method, the first 8 sidebands are included in the calculation. The result is viewed below in Figure 32. The blue line represents the benchmark case. The red line shows the damage indicator of the 1 mm damage case with respect to the pristine case and the yellow line the 2.5 mm damage case with respect to the pristine case. In the ideal situation, the yellow line should yield the highest value on the damage indicator, the red line the second highest and the blue line the lowest over the entire frequency range, this is the case for most frequencies.

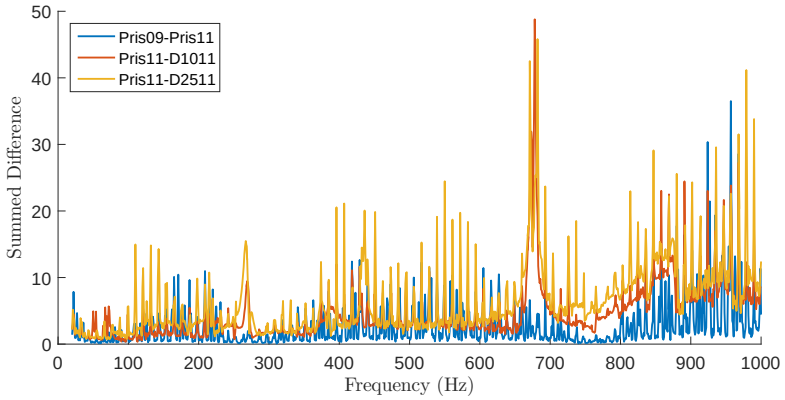

Figure 32: Unfiltered results of benchmark case

One observation that immediately stands out from the results is that many peak values appear very periodically. The spikes in the experimental results of the damage cases are all linear combinations of 11 Hz, or a tenfold of the scan rate of 1.1 Hz. This can be explained as scan rate harmonic speckle noise. Martarelli and Ewins published on speckle noise related to the scan rate in 2006 [24]. It was stated that at the scan rate and its harmonics, noise is expected in the signal. If noise is introduced by the scan rate, and at the scan rates harmonics, then all measurements that are a multiple of 1.1 will be effected. The beam is excited at integer frequencies, so the first scan rate harmonic that occurs is at 11 Hz. Because of the discrete sideband operations in the damage indicator, the scan rate harmonics coincide precisely with the sidebands at that harmonic excitation frequency. The noise at exactly these frequencies contribute to a changing spectrum shape on which the damage indicator is based, resulting in a higher damage indicator value. The trend of the damage indicator result would be more clear without this speckle noise. Therefore these peaks should be filtered out. The periodicity of these peaks can be more clearly seen when a FFT of the damage indicator result itself is taken over the frequency range. The result for the 1 mm damage case is viewed in Figure 33. The peaks can immediately be distinguished, however, the x-axis needs to be modified to present the correct frequencies.

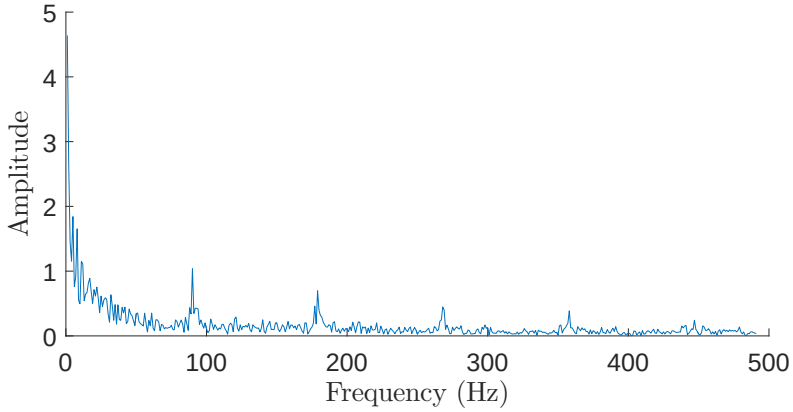

Figure 33: FFT of indicator graph for the 1 mm damage case

As implemented above, an FFT takes a time signal and transforms it to a frequency spectrum of that signal. In this case, the input is in the frequency domain, so the output should be modified. The input is treated as a time signal of 1 second, the measurements range from 20 Hz to 1000 Hz, this means 981 sample point. So a 'sampling frequency' of 981 Hz. An FFT of such a signal results cuts off at a Nyquist frequency of half that, 491 Hz. The first peak appears at 90 Hz in the unmodified FFT. This means a period of $\frac{1}{90}$ s. This multiplied with the number of samples: 981, equals nearly 11 Hz. When the x-axis is modified to represent that, the peaks at the 11 Hz

harmonic become clear, as seen in Figure 34. The graph is now also cut off at 491 Hz, the expected Nyquist frequency. To make the graph smoother, notch filters were placed at these harmonics. This will make the behaviour of the damage indicator more clear. The filtered FFT is also plotted in Figure 34. This gives a better sense of the general, underlying behaviour of the damage indicator.

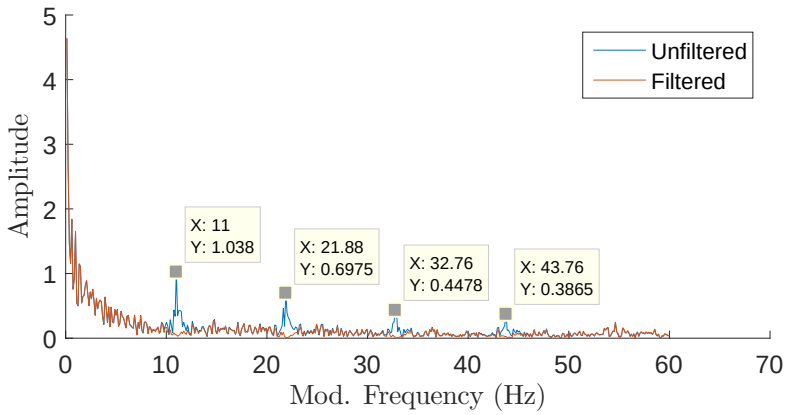

Figure 34: Filter effect of FFT of 1 mm damage case with modified x-axis

These filters are also applied to the benchmark case. An important thing to note is that the comparison of the pristine case consists of a scan at 1.1 Hz and a scan at 0.9 Hz, meaning that the speckle noise harmonics at 9 Hz should also be filtered as well. The result of the filtered damage indicators is shown in Figure 35.

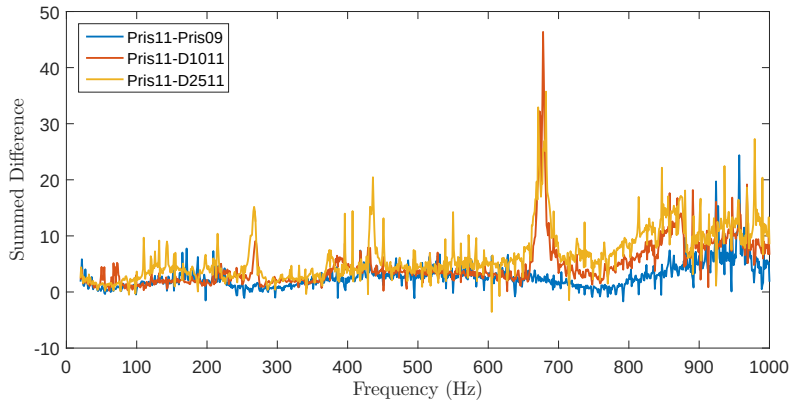

Figure 35: Filtered experimental results of damage indicator

5.4 Comparison to numerical

In the introduction to this section, the hypothesis was made that the numerical results would not be the same as the experimental results. In this section, the experimental part is compared to the numerical part. The FRF and the damage indicator are compared in Figure 36, where the 1 mm damage case is plotted over the FRF up to 1000 Hz. There are a few frequencies that stand out, the peaks in the indicator at 267 Hz and 678 Hz. The relevance of these frequencies can be explained when compared to the FRF.

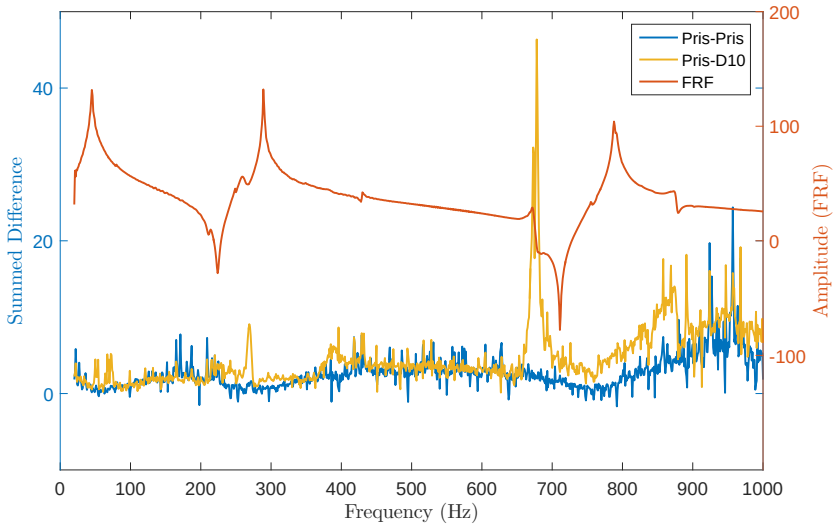

Figure 36: Filtered indicator results (left axis) in relation to the FRF (right axis)

Both peaks in the damage indicator are close to the anti-resonances at 225 Hz and 717 Hz, however both also show a small peak in the FRF around these actual frequencies. These are speculated to be torsional components. The FRF does not align well with the analytically calculated eigen-frequencies, shown in Table 9. A contributing factor to this is that it was found that the rig build to clamp the frame is not perfectly rigid in this frequency range. Some compliance was found in the system that has influence on the eigen-frequencies.

Table 9: Eigen-frequency comparison

ω	Analytical (Hz)	Experimental (Hz)
1	51	45
2	319	291
3	889	795

There is some conflicting information. The low noise between 700 and 800 Hz for the Pristine case indicates the resonance, namely high signal-to-noise ratio due to the large excitation amplitude. This does not truly line up with the peak of the third eigen-frequency in the FRF, like it does in the numerical analysis. This also seems to be the case for the second eigen-frequency. If the FRF were to shift left to accommodate for this, the peak in the indicator does line-up with the second anti-resonance, but the first anti-resonance would not line-up with the peak at 267 Hz in the D10T damage case.
The general behaviour of the pristine case, compared to another pristine case correlates very well to the numerical results with added random noise. The noise at frequencies between the resonances result in a relatively high damage indicator. At and around the eigen-frequencies, the signal-to-noise ratio increases and the damage indicator becomes lower. This shows up less in the range between 20 and 1000 Hz in the numerical results, however the overall behaviour is similar, as displayed by the blue line in Figure 27.
Another difference is found in the overall shape between the damage indicator results of the experimental and numerical analyses. This is because of a fundamental difference in the way the experiments are conducted and the simulation is performed. In the simulation, a set force magnitude is applied to all frequencies, while in the experiment, the force magnitude differs for every frequency. This is part of the reason why the indicator had to include some sort of normalisation of the force input level. This is also why the signal to noise ratio is so high for the first 1000 Hz in the model.

6 Conclusions

In this thesis, an existing measurement method in the form of Continuous Scanning LDV (CSLDV) was used to devise a novel way of performing structural health monitoring. The literature study reviews that the CSLDV method has the potential for rapid damage detection. Where most current methods reconstruct the operational deflection shape from the CSLDV output signal. This method directly uses the spectral sidebands extracted from the CSLDV method.
A finite element model of the beam is made and the dynamic behaviour of the beam is analysed. By keeping the simulation to a two-dimensional problem, the spatial information obtained from the method is minimal.
A strain analysis indicated a higher sensitivity at the anti-resonance than at eigen-frequency. It seems that the anti-resonance implies an additional constraint in cantilever applications, which causes a higher sensitivity to damage. Where previous literature is only interested in eigen-frequencies, a potential application for use in SHM was suggested.
Multiple damage indicators were formulated in pursuit of a sensitive and robust indicator. The indicators where applied to the numerical results. The RASTAR method, which tracks the contribution per sideband to the sum of the sidebands in a spectrum and compares it to a known condition, was found to be able to measure the change in dynamic behaviour as a result of the stiffness degradation. The method does this independent of the excitation force. The indicator still performed well when noise was added to the simulation.
The method was then validated by conducting experiments with a pristine case and two damage cases. In the numerical simulation, it was revealed that the anti-resonances are the most sensitive to the applied damage using the RASTAR method. Although some spikes in sensitivity were observed, the experimental work could not definitively validate this. It did demonstrate that the method yields logical results. An increase in severity returns an increase in the damage indicator value.
The goal of the study was to develop a diagnostic method that makes use of solely the spectral sidebands of the CSLDV method. The RASTAR method was able to detect a damage in the form of a 1x1x30 mm transverse cut in a 400x10x30 mm beam. The method is considered a robust and successful damage indicator for application in cantilever structures.

7 Recommendations & Future work

This section provides an outlook on future application of the method. After which, a list of recommendations on future work is presented.
For future application of the method it is recommended to be applied to cantilever structures, excited in anti-resonance. This frequency seems to be the most sensitive to damage. Another frequency of interest is the eigen-frequency. The high signal-to-noise ratio at the eigen-frequency shows the lowest value on the benchmark damage indicator. At that frequency, a false positive indication of damage is less likely to occur. For small expected damages this could be advantageous. So a combination of excitation frequencies should be employed.
A dynamic maintenance scheme can be implemented using the RASTAR method by evaluating the damage indicator on a short time interval. Before implementation, tests should be done to find an indicator value that triggers further inspection when reached. This should be established for every test frequency that will be applied. The rapid method is able to pick up small transverse damages, so it should be implemented in structures where this damage type is most likely to occur.
For future work, this thesis provides insight in the use of the spectral sidebands of the CSLDV method for SHM purposes. These recommendations are listed below:

- A very brief strain analysis indicated the use of anti-resonances for application in measuring structural health. A solid conclusion on the sensitivity to damage at anti-resonance for cantilever structures could not be drawn based on the experimental work. The novelty of the potential of the use of anti-resonances should be further investigated.

- The inclusion of the third dimension in the analysis is a logical next step. The laser is capable of scanning in both x- and y-direction, and more spatial information can be obtained. Evaluating the damage using the RASTAR method is advised to be implemented separate for x- and y-scan rates respectively. This should allow for distinction in bending and torsional components to the damage. Certain damages are expected to effect certain deflection shapes more heavily and might therefore be more sensitive.

- The method should also be tested on beams with varying damage and excitation locations. A relation between the damage location and the sensitivity to the damage indicator is apparent, looking at the strain energy behaviour through the beam. This could be combined with the analysis of the anti-resonances. Since the eigen-frequencies do not change with the excitation frequency, but the anti-resonances (measured at excitation location) do vary.

- Another aspect that should be studied is the effect of the scan rate, an optimum should be found where the speckle noise has a minimal impact on the experimental results. There could also be a scan rate that is more sensitive overall, or more sensitive at certain excitation frequencies. Also the number of sidebands to be included could be varied per frequency, this should reduce noise by only taking the most important sidebands in consideration.

- On the current work, the results from the experiments are not as similar to the analytical or the numerical results as expected. Repeating the experiments could be done with a more rigid structure. The damage should be applied while the beam is in the rig, to prevent occurrence of difference in modal behaviour other than that due to the damage. This should yield a better FRF, and probably more agreement with the numerical simulation.

References

[1] Chopra, I. Review of State of Art of Smart Structures and Integrated Systems. *AIAA JOURNAL 40*, 11 (2002).

[2] Johnson, T. J., Brown, R. L., Adams, D. E., and Schiefer, M. Distributed structural health monitoring with a smart sensor array. *Mechanical Systems and Signal Processing 18*, 3 (5 2004), 555–572.

[3] Sierra-Pérez, J., Torres-Arredondo, M. A., and Güemes, A. Damage and nonlinearities detection in wind turbine blades based on strain field pattern recognition. FBGs, OBR and strain gauges comparison. *Composite Structures 135* (1 2016), 156–166.

[4] Abry, J., Bochard, S., Chateauminois, A., Salvia, M., and Giraud, G. In situ detection of damage in CFRP laminates by electrical resistance measurements. *Composites Science and Technology 59*, 6 (5 1999), 925–935.

[5] McCormick, N., and Lord, J. Digital Image Correlation. *Materials Today 13*, 12 (12 2010), 52–54.

[6] Avril, S., Bonnet, M., Bretelle, A.-S., Grédiac, M., Hild, F., Ienny, P., Latourte, F., Lemosse, D., Pagano, S., Pagnacco, E., and Pierron, F. Overview of Identification Methods of Mechanical Parameters Based on Full-field Measurements. *Experimental Mechanics 48*, 4 (8 2008), 381–402.

[7] Mian, A., Han, X., Islam, S., and Newaz, G. Fatigue damage detection in graphite/epoxy composites using sonic infrared imaging technique. *Composites Science and Technology 64*, 5 (4 2004), 657–666.

[8] Pastor, M., Balandraud, X., Grédiac, M., and Robert, J. Applying infrared thermography to study the heating of 2024-T3 aluminium specimens under fatigue loading. *Infrared Physics & Technology 51*, 6 (10 2008), 505–515.

[9] Jacquot, P. Speckle interferometry: A review of the principal methods in use for experimental mechanics applications. *Strain 44* (02 2008).

[10] Reddy Guntaka, S., Hertwig, M., Flemming, T., and Usinger, R. Speckle interferometry for detection of subsurface damage in fibre-reinforced composites Speckle interferometry for detection of subsurface damage in f i bre-reinforced composites. *Meas. Sci. Technol 5* (1994), 100–104.

[11] De la Torre, I. M., Hernández Montes, M. d. S., Flores-Moreno, J. M., and Santoyo, F. M. Laser speckle based digital optical methods in structural mechanics: A review. *Optics and Lasers in Engineering* (2015).

[12] Castellini, P., Martarelli, M., and Tomasini, E. Laser Doppler Vibrometry: Development of advanced solutions answering to technology's needs. *Mechanical Systems and Signal Processing 20*, 6 (8 2006), 1265–1285.

[13] Martarelli, M. *Exploiting the Laser Scanning Facility for Vibration Measurements*. PhD thesis, University of London, May 2001.

[14] Stanbridge, A. B., and Ewins, D. J. Modal testing using a scanning laser Doppler vibrometer. *Mechanical Systems and Signal Processing* (1999).

[15] Chen, D. M., Xu, Y. F., and Zhu, W. D. Non-model-based multiple damage identification of beams by a continuously scanning laser Doppler vibrometer system. *Measurement: Journal of the International Measurement Confederation* (2018).

[16] Khan, A. Z., Stanbridge, A. B., and Ewins, D. J. Detecting damage in vibrating structures with a scanning LDV. *Optics and Lasers in Engineering 32* (2000), 583–592.

[17] Di Maio, D., Zampognaro, N., Zang, C., and J. Ewins, D. Effect of vibration excitation locations on structural damage detection using the csldv technique: simulation and testing. In *Proceedings of SPIE - The International Society for Optical Engineering - art. no. 63450O* (06 2006).

[18] Di Maio, D. Use of continuous scanning LDV for diagnostics. In *Conference Proceedings of the Society for Experimental Mechanics Series* (2016).

[19] Rucevskis, S., and Wesolowski, M. Identification of Damage in a Beam Structure by Using Mode Shape Curvature Squares. *Shock and Vibration 17*, 4-5 (2010), 601–610.

[20] Di Maio, D. Damage monitoring using continuous scanning LDV methods: numerical approach. In *Optical Measurement TEchniques for Structures & Systems III* (Antwerp, Belgium, 2015), J. Dirckx, Ed., pp. 61–71.

[21] Ramesh, L., Rao, P., Kumar, K., and Prasad, D. Experimental and Finite Element Model Analysis of an un-cracked and cracked Cantilever beam. *International Journal of Advanced Research in Science, Engineering and Technology 3*, 1 (2016).

[22] Ostachowicz, W., and Krawczuk, M. Analysis of the effect of cracks on the natural frequencies of a cantilever beam. *Journal of Sound and Vibration 150*, 2 (10 1991), 191–201.

[23] Allemang, R. J. The modal assurance criterion - Twenty years of use and abuse. *Sound & vibration 37* (7 2003), 14–23.

[24] Martarelli, M., and Ewins, D. J. Continuous scanning laser Doppler vibrometry and speckle noise occurrence. *Mechanical Systems and Signal Processing 20*, 8 (11 2006), 2277–2289.

A FRF

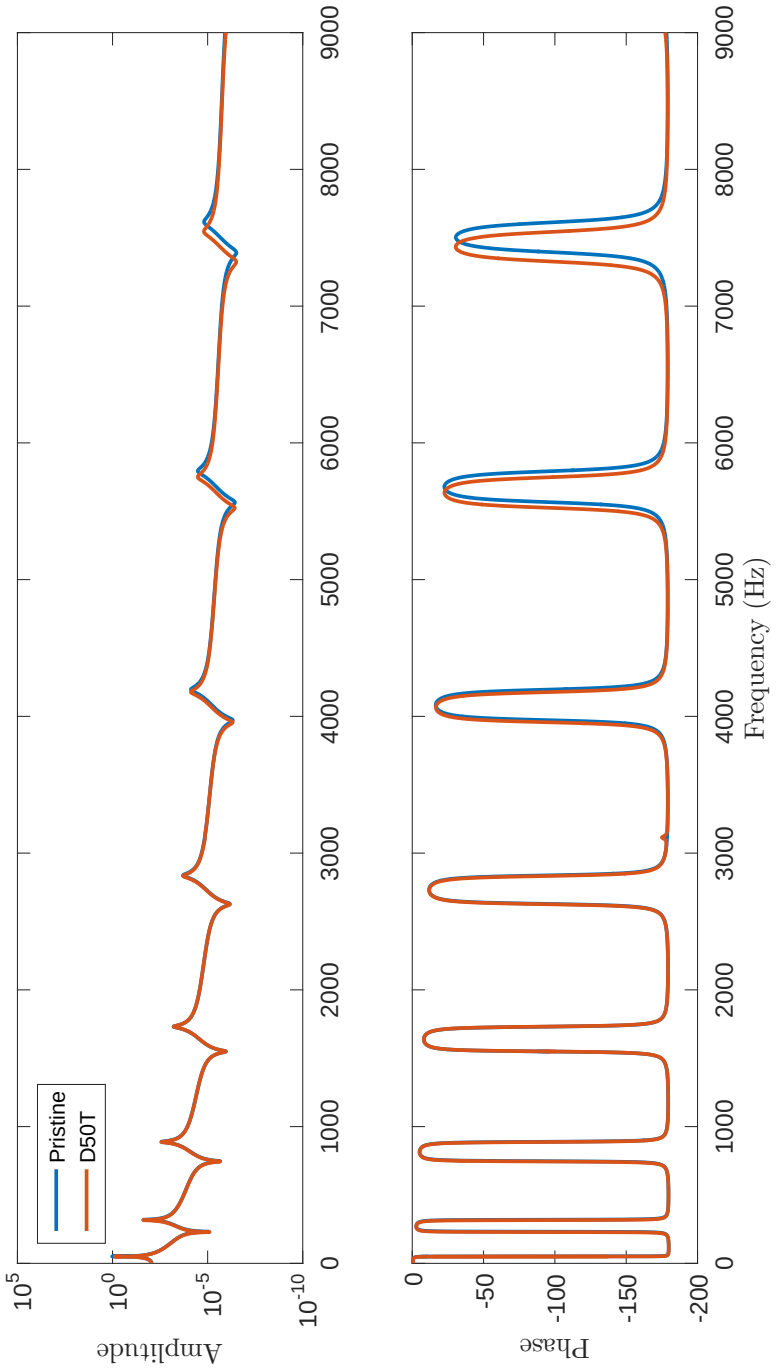

Figure 37: Frequency Response Function of P & D50T

B Conference Proceeding

This paper was submitted to be published in the A.I.VE.LA. conference proceedings of 2018. The findings of the paper were presented in Ancona, Italy at the conference on June 20th.

Diagnostics based on continuous scanning LDV methods: numerical study

S Bruinsma, D Di Maio, T Tinga

Dynamics Based Maintenance, Department of Engineering Technology, Horst 2, 7522 LW, Enschede, The Netherlands

Abstract. This paper presents a research work on diagnostics using continuous scanning laser methods. Structural Health Monitoring based on laser vibrometry can exploit the ability of a scanning laser to measure vibration responses remotely both regarding temporal and spatial resolution. Therefore, it can be a powerful approach for rapid damage detection of components presenting an unhealthy dynamic behaviour. The work is focused on numerical analysis of a cantilever beam which is subjected to damage of different severity levels. The severity will be measured regarding response phase shift for a fixed excitation frequency. The simulated nodal responses of the surface being scanned by a laser beam are selected and used for simulating the spectral responses obtained from CSLDV methods. The main objective of this work is to determine the structural integrity based on an indicator obtained by referencing the relative spectral sidebands between a pristine and damage condition.

1. Introduction

In recent years, durability and extension of life of components has become an important topic of research. Structural Health Monitoring (SHM) focuses on detection of unhealthy dynamic behaviour as damage occurs and propagates in the structure. The early detection of damage is highly interesting for for maintenance in the industry, which supported research for better diagnostic tools. These consist of destructive and non-destructive methods. Obviously, non-destructive methods are preferred, as these are most applicable in the industry for SHM. A conventional way of testing is to apply strain gauges to the component. However, these cannot be placed on rotating shafts, for example. Also, the fastening methods cannot always be applied due to high operating temperature. This can be omitted by using a non-destructive and non-contact measurement technique. Most of these techniques use either laser light, such as Holography, Speckle interferometry and Scanning Laser Doppler Vibrometry (SLDV), or a camera, like Digital Image Correlation (DIC).

DIC uses a camera and image processing to obtain dynamic information[1]. DIC requires surface preparation and a lot of post processing to obtain results on the strain. Holography is a expensive method that allows for comprehensive measurements [3]. The downside for the industry is that the part needs to be isolated and placed in this large and finely tuned test set-up, increasing downtime of the system. Interferometry needs a similar sterile environment to do the measurements [9]. SLDV is a more robust approach that allows for the possibility of in-situ measurements [2]. Continuous SLDV strengthens this application by making it a very fast measurement method.

This paper focuses on Continuous SLDV, which main advantage is fast acquisition of both spacial and temporal information. CSLDV uses a laser that scans a vibrating structure. The time signal from a sinusoidal line scan can be modulated to a frequency spectrum [4], which can be used for SHM. The level of depth in damage detection is categorised in 4 levels, as explained in [5], the definition of the different levels are displayed in Table 1. Most of the current research with this technique is on locating the damage [6], which is quantified as SHM level 2. To exploit its main advantage of speed, the level of SHM is reduced to 1 in this study, where only the detection of damage is pursued.

Table 1: Level of SHM

Level 1	Determination that damage is present
Level 2	Determination of the geometric location of the damage
Level 3	Quantification of the severity of the damage
Level 4	Prediction of the remaining service life

A numerical study is undertaken, analysing a cantilever, aluminium beam. The prismatic beam is subjected to an oscillating force at the free end. The goal of the study is to determine the sensitivity of the CSLDV method to introduced damage. To accomplish this, different approaches to defining a damage criterion are taken.

2. Method

In this chapter the methodology of the research is presented. First the construction of the model is described. The model is checked and the sensitivity to the damage is analysed. This is then used to define damage indicators that are sensitive enough to show propagation of damage.

2.1. Numerical Model

Researching the viability and sensitivity of this method is done on a simple geometry, a prismatic, cantilever beam. The dimensions of the beam are 0.4x0.04x0.01 m (l,w,h) or (x,z,y). The beam is modelled in Finite Element Program ANSYS Mechanical APDL 16.2. The beam is modelled with 200x20 (x,y) rectangular SHELL181 elements. Only membrane bending is used, and full integration. All nodes are locked in z-direction, one end is fixed in y- and x-directions as well. At the other end, an excitation force is applied in y-direction. The harmonic response is simulated from 1 to 9000 Hz with a frequency step of 1 Hz. The model shows good correspondence to analytical eigen frequency calculations. The first six eigen frequencies are compared in Table 2.

Table 2: Comparison Analytical and Numerical

	ω_1	ω_2	ω_3	ω_4	ω_5	ω_6
Analytical (Hz)	51.04	319.9	895.4	1755	2901	4334
Numerical (Hz)	51	319	889	1731	2837	4196
Error (%)	<0.1	0.3	0.7	1.4	2.2	3.2

The prismatic beam has a consistent width (z-direction) of elements of 0.04 m. Damage is introduced to the model by reducing the width of the elements, which results in a stress concentration around the damaged elements. This way of modelling allows for a wide variety of elaborate damage cases, such as delamination and interlaminar cracks. In this study, a simple damage case is defined: a transverse cut, or saw cut. The transverse cut is placed at 0.04 m from the root, starting on the lowest row of elements, made in three severities. The most extreme case is the 50% damage case, where the cut is 0.005 m, thus half the thickness (in y-direction), which corresponds to 10 elements with reduced width. Furthermore, 25% of the thickness and 10% of the thickness are evaluated, corresponding to 5 and 2 elements respectively.
The ODS for all frequencies is extracted and a curve is fitted through the shape using the $polyfit$-function in MATLAB. The x-coordinates are transformed between -1 and 1, to allow for simulation of the CSLDV time signal. This time signal is the result of equation 1, from [7].

$$v(t) = \sum_{n=0}^{p} V_{Rn} \cos^n(\Omega t) \cos(\omega t) \tag{1}$$

Where p is the order of the polynomial used to describe the ODS, V_R is the real part of the polynomial coefficients, Ω is the scan frequency of the CSLDV (in this paper 1.1 Hz.). ω is the excitation frequency.

2.2. Sensitivity

To establish an indicator for the damage severity levels in relation to the vibration modes three FRFs were simulates for the damage cases. The crack is placed close to the root of the beam (10% the beams length, measured from the clamped end). The 50% transverse crack is 2 mm wide and 5 mm in length, which causes a frequency shift of less than 1% from the pristine natural frequency for almost all eigen frequencies, both FRFs from pristine and damage cases are presented in Figure 1.

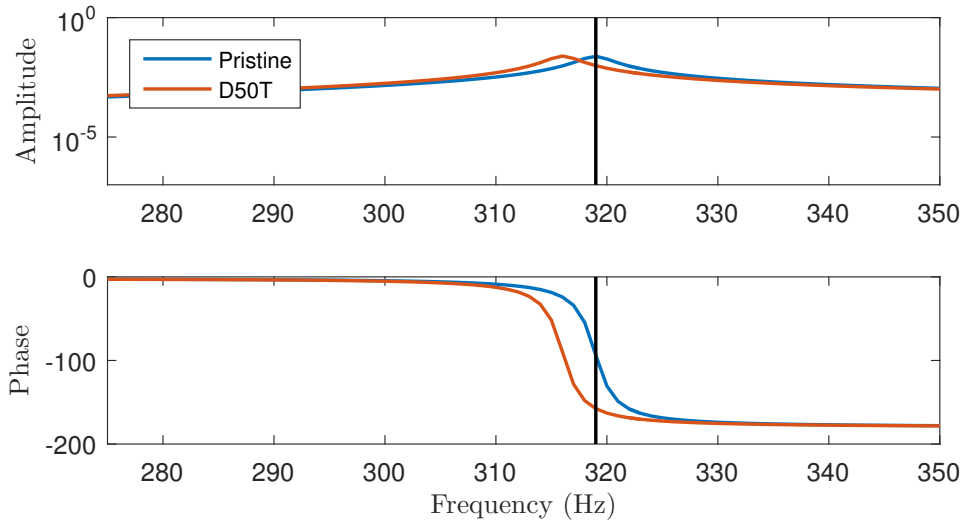

Figure 1: FRF of Pristine & D50T

This behaviour is as expected, the applied damage to the structure reduces the stiffness in the beam [8]. The eigen frequency is proportional to k/m, where k is stiffness and m is mass. The severity of the damage is commonly measured in the frequency shift of the eigen frequencies. However, for a given structural damping, the response phase of a damaged structure shows much larger deviation from a pristine condition. As seen in Figure 1 this shows a higher sensitivity due to phase behaviour at a fixed frequency, such as the eigen frequency. Table 3 shows both the frequency shift and the phase shift with respect to the resonant frequency.

Table 3: Response to damage severity

	Frequency (Hz)				Phase shift at ω^P (deg)			
Eigen	P	D10T	D25T	D50T	P	D10T	D25T	D50T
ω_1	51	51	50	50	-79	-134	-164	-170
ω_2	319	318	317	316	-94	-117	-145	-158
ω_3	889	889	888	887	-92	-97	-107	-117
ω_4	1731	1731	1731	1731	-96	-94	-92	-91
ω_5	2837	2837	2835	2833	-94	-97	-105	-115
ω_6	4196	4193	4184	4178	-96	-108	-131	-142
ω_7	5794	5785	5766	5750	-100	-120	-148	-157
ω_8	7616	7602	7571	7546	-104	-127	-154	-163

These differences are visualised in Figures 2 & 3. Where the found values are normalised to the pristine case and a relative shift is plotted.

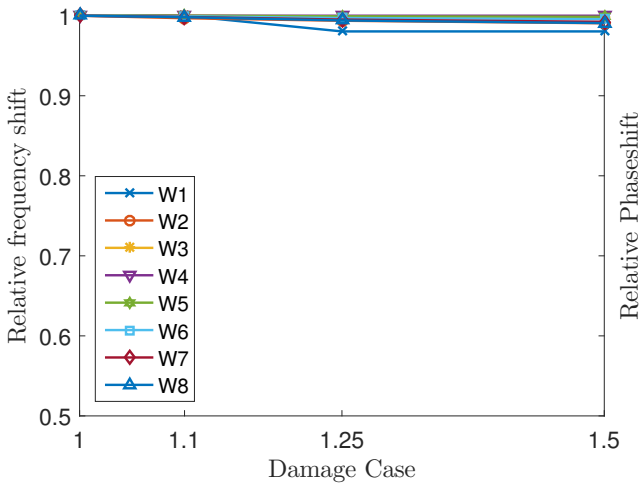

Figure 2: Frequency shift

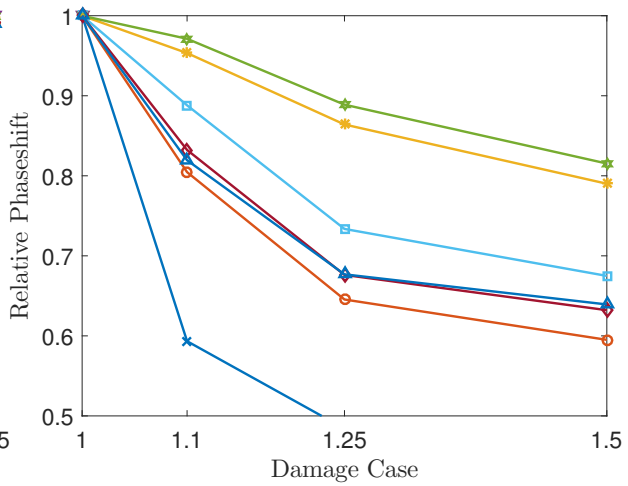

Figure 3: Phase shift

Based on such indicator, the most sensitive modes to the damage can be highlighted and closely observed during the next phase of the research.

2.3. signal processing

All the ODSs simulated by the FEM are curve-fitted with a 15^{th} order polynomial. LDV output modulated signals are generated and processed by dFFT. the dFFT is discretised at the excitation frequency and subsequently at interval of the scan frequency, as in [10]. This results in a middle amplitude with sidebands at equal distances. The amount of sidebands is equal to the amount of polynomial coefficients. The magnitude of these sidebands carry the spatial information of the ODS. Meaning that the distribution of the amplitude of each sideband is characteristic for that system at that specific frequency.
When damage is introduced to the beam, this characteristic distribution of amplitudes over the sidebands differs, as seen in Figure 4. This is more clearly seen when a log scale on the y-axes is used.

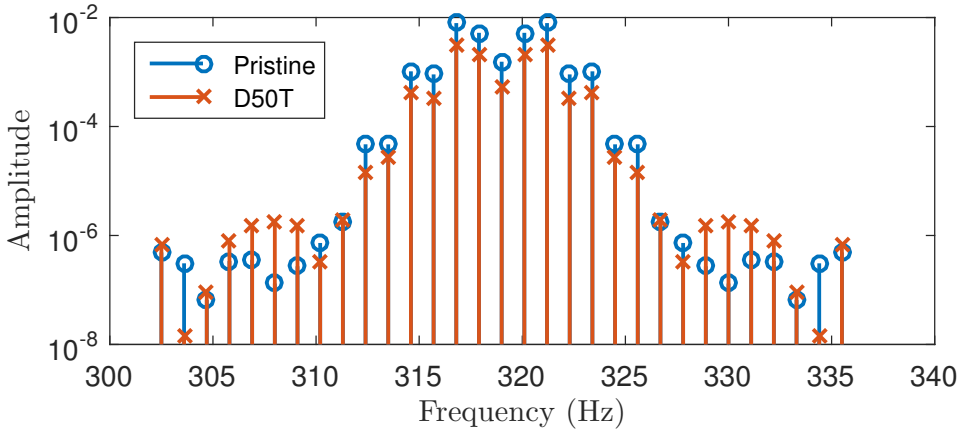

Figure 4: dFFT at 2nd eigen frequency (P and D50T)

As already introduced, 15 coefficients are used for the polynomial evaluation. However, the ODSs require a different amount of coefficients, less are needed if the shape is simple like the first bending mode. The minimal number of coefficients needed to adequately describe the ODS is investigated at the eigen frequencies of the beam. This is done by checking the MAC value of the fit for increasing number of polynomial coefficients.

Table 4: Minimal Nr. of Coefficients (MAC = 0.999)

eigen freq	1	2	3	4	5	6	7	8
Nr. of coeff.	2	4	5	8	9	10	13	14

So for the second eigen frequency (319 Hz), only 4 coefficients are required to construct the ODS. This results in many near-zero coefficients, as can be seen in Figure 4. It is important to note that the amplitude of the sidebands does not simply shift up or down, this would mean that is is the same ODS but at lower or higher (excitation) amplitude. In the higher order sidebands, it is clear that this is not the case. However, as said before, these sidebands do not hold much meaning since the amplitudes are near-zero. So it becomes critical to analyse the difference of the first four sidebands as well.
The following two subsections will provide an attempt to quantify the deviation between a pristine and damaged case by developing an indicator to rank the damage severity with respect to mode shapes.

2.4. Fingerprint

A method to observe the difference between a pristine and damaged case is to create a so-called *fingerprint*. Every sideband is scaled by the one measured at the excitation frequency (ω). This is done for each sideband (i) following equation 2.

$$FPA_i(\omega) = SBA_i(\omega + \Omega \cdot i)/SBA(\omega) \tag{2}$$

FPA_i is the fingerprint (normalised) amplitude of sideband i, obtained by dividing sideband amplitude SBA_i over the excitation or middle amplitude. Hence, both pristine and damaged case will present a typical fingerprint.

2.5. Sideband polynomial

As described before, the spectral sideband amplitudes are related to the polynomial coefficients of the wave shape of the ODS. The relation between the sideband amplitude and the polynomial coefficient is used to define a damage indicator. The difference in sideband amplitudes between the pristine case and damage case is related to the change in ODS, which is a polynomial function. The first sideband corresponds to the linear term, the second to the quadratic, and so on. This is integrated in the damage indicators defined below.

$$\mathrm{DIP}_1 = \sum_{i=1}^{n} SBA^i_{Pi} - SBA^i_{Di} \tag{3}$$

$$\mathrm{DIP}_2 = \sum_{i=1}^{n} SBA_{Pi} \cdot i^i - SBA_{Di} \cdot i^i \tag{4}$$

$$\mathrm{DIP}_3 = \sum_{i=1}^{n} SBA_{Pi} \cdot i^{i-1} - SBA_{Di} \cdot i^{i-1} \tag{5}$$

$$\mathrm{DIP}_4 = \sum_{i=1}^{n} (SBA_{Pi} \cdot i^i - SBA_{Di} \cdot i^i) \cdot \omega \tag{6}$$

Where SBA_{Pi} is the i^{th} sideband of the Pristine case. ω is the excitation frequency. This is done for a number of sidebands up to 15.

3. Results

In this section the results of the damage indicators described in the section above are shown.

3.1. Fingerprint

The fingerprint method yields a characteristic shape for the pristine case and the damaged case as seen in Figure 5. These shapes are referred to the fingerprint of the beam.

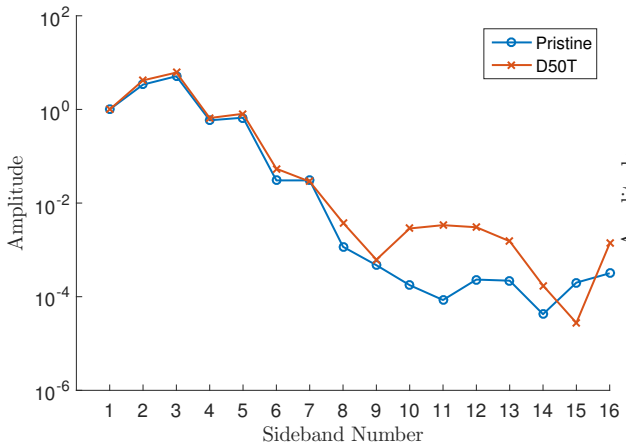

Figure 5: Fingerprint method

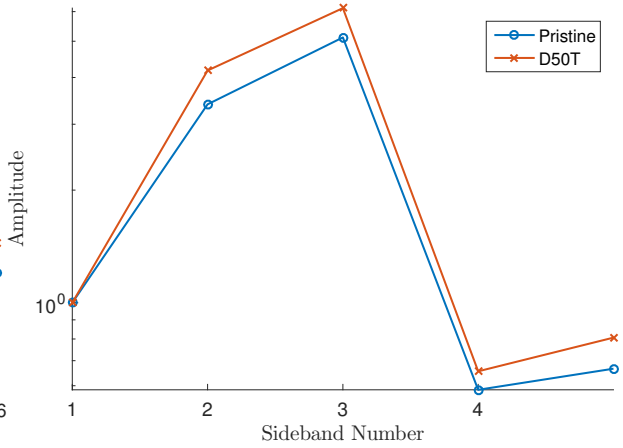

Figure 6: Fingerprint zoom

As can be seen in Figure 5, the higher order sidebands show most difference in relative amplitude. These are however most difficult to detect and in absolute numbers have very low value. The difference is visible in the first four sidebands when these are observed, see Figure 6. Detecting damage from this Figure can be done, but assigning a scalar value would be preferable. One possible damage criterion to obtain from this is the mean square error between the two fingerprints. The mean square error is 0.1 for the second eigen frequency. When this is evaluated over the entire frequency range, some spikes appear, as seen in Figure 7.

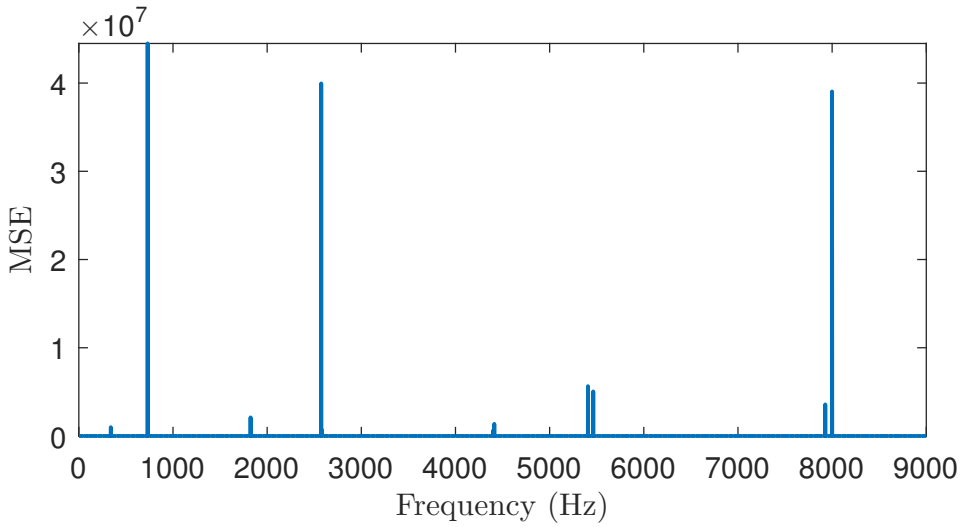

Figure 7: Mean Square Error for all frequencies

The reason for these spikes is investigated and can be explained with Figure 8.

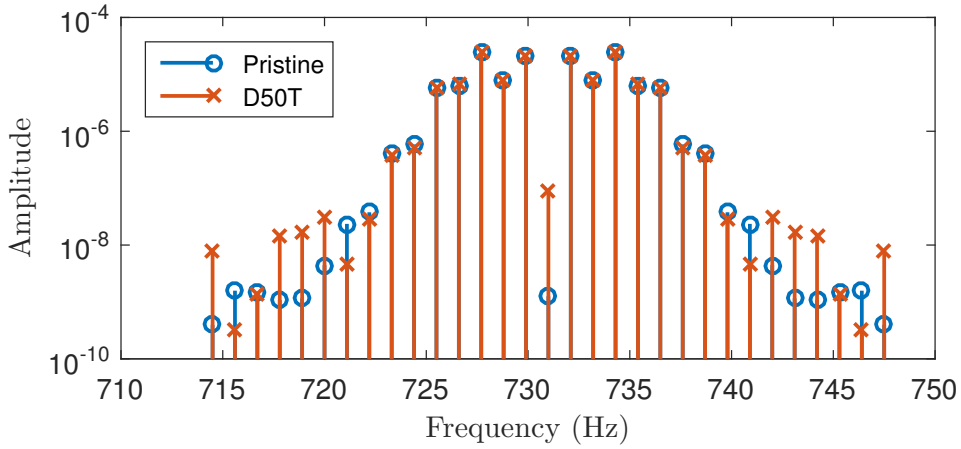

Figure 8: Problem case Mean square error

From Figure 8, it can be concluded that a large difference in the middle amplitude results in unusually large Mean Square Errors.

3.2. Sideband polynomial

The result of the sideband polynomial methods are damage indicators that are highly dependent on the frequency and the method does not normalise the sideband amplitudes. Therefore the indicators only show meaningful difference around the eigen frequency, where the vibration amplitudes are generally high. Furthermore, at the anti-resonance a spike occurs, because vibration amplitudes are very small. The frequency dependency built in to equation 6 shows more consistency regarding the value indicated by the damage severity. However, at any frequency away from the eigen frequency, the damage is not indicated. The frequency dependent indicator is view in Figure 9.

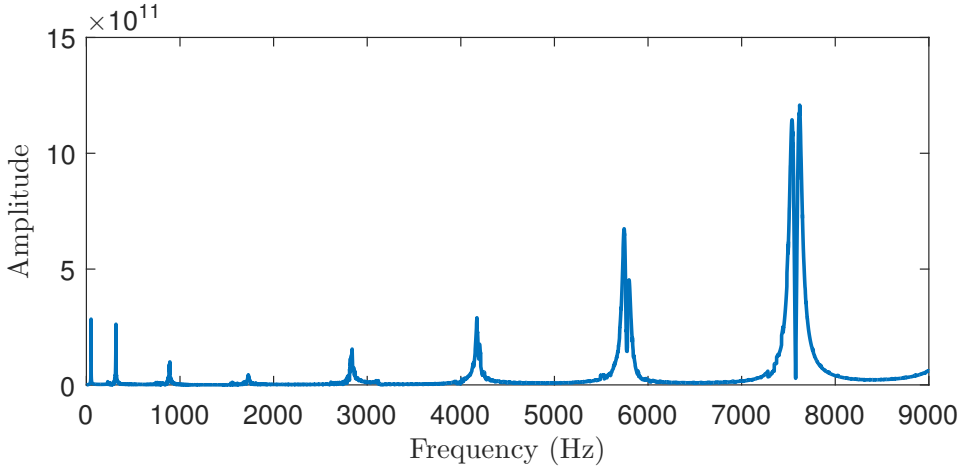

Figure 9: Sideband Polynomial Indicator

4. Conclusions

In this study, the use of the CSLDV method for SHM purposes is explored. The method is fast in assessing the ODS of a beam by using the FFT frequency spectrum. This spectrum has a characteristic shape that can be used as a reference. The fingerprint method shows potential in detecting the difference between a damaged and pristine spectrum. However, this method shows inconsistent behaviour over the frequency range, making it an unsuitable approach for this application. The other methods suffer from the same problem, a very small window of frequencies is found where a useful value can be extracted. This makes it heavily model dependent and not much more useful than the current technique of measuring the shift in eigen frequency.

The problem with the fingerprint method is that the indicator is too dependent on the amplitude of one of

the sidebands used for the calculation and therefore makes the indicator unstable. The approach of relative contribution of the sidebands does hold. When fixed frequencies are observed, the overall amplitude changes when damage is introduced, as seen in the FRF. From an application point of view, this is also the case when not the exact same force is applied. So making the sidebands a relative, or normalised factor would make it comparable again.
Instead of normalising the sideband amplitudes to one sideband, it would be better to assign partial contributions to the sidebands in relation to all other sidebands. This is further investigated, mathematically and experimentally, in an upcoming paper.

References

[1] Stéphane Avril, Marc Bonnet, Anne-Sophie Bretelle, Michel Grédiac, François Hild, Patrick Ienny, Félix Latourte, Didier Lemosse, Stéphane Pagano, Emmanuel Pagnacco, and Fabrice Pierron. Overview of Identification Methods of Mechanical Parameters Based on Full-field Measurements. *Experimental Mechanics*, 48(4):381–402, 8 2008.

[2] P. Castellini, M. Martarelli, and E.P. Tomasini. Laser Doppler Vibrometry: Development of advanced solutions answering to technology's needs. *Mechanical Systems and Signal Processing*, 20(6):1265–1285, 8 2006.

[3] I. Manuel De la Torre, María del Socorro Hernández Montes, J. Mauricio Flores-Moreno, and Fernando Mendoza Santoyo. Laser speckle based digital optical methods in structural mechanics: A review. *Optics and Lasers in Engineering*, 2015.

[4] Dario Di Maio. Use of continuous scanning LDV for diagnostics. In *Conference Proceedings of the Society for Experimental Mechanics Series*, 2016.

[5] Z A Jassim, N N Ali, F Mustapha, and N A Abdul Jalil. A review on the vibration analysis for a damage occurrence of a cantilever beam. *Engineering Failure Analysis*, 31:442–461, 2013.

[6] Jeong Tae Kim, Yeon Sun Ryu, Hyun Man Cho, and Norris Stubbs. Damage identification in beam-type structures: Frequency-based method vs mode-shape-based method. *Engineering Structures*, 2003.

[7] Milena Martarelli. Exploiting the Laser Scanning Facility for Vibration Measurements. 2001.

[8] W.M. Ostachowicz and M. Krawczuk. Analysis of the effect of cracks on the natural frequencies of a cantilever beam. *Journal of Sound and Vibration*, 150(2):191–201, 10 1991.

[9] Sridhar Reddy Guntaka, Manfred Hertwig, Torsten Flemming, and Ralf Usinger. Speckle interferometry for detection of subsurface damage in fibre-reinforced composites Speckle interferometry for detection of subsurface damage in f i bre-reinforced composites. *Meas. Sci. Technol*, 5:100–104, 1994.

[10] A. B. Stanbridge and D. J. Ewins. Modal testing using a scanning laser Doppler vibrometer. *Mechanical Systems and Signal Processing*, 1999.